Biomaterials 293 (2023) 121978

Contents lists available at ScienceDirect

Biomaterials

journal homepage: www.elsevier.com/locate/biomaterials

Chitosan and HPMCAS double-coating as protective systems for alginate microparticles loaded with Ctx(Ile^{21})-Ha antimicrobial peptide to prevent intestinal infections

Cesar Augusto Roque-Borda [a,**], Mauro de Mesquita Souza Saraiva [b], Wagner Dias Macedo Junior [c], José Carlos Estanislao Márquez Montesinos [d], Andréia Bagliotti Meneguin [a], Anna Beatriz Toledo Borges [a,1], Edson Crusca Junior [e], Saulo Santesso Garrido [e], Adriana Maria de Almeida [b], Reinaldo Marchetto [e], Marlus Chorilli [a], Angelo Berchieri Junior [b], Silvio Rainho Teixeira [c], Fernando Rogério Pavan [a], Eduardo Festozo Vicente [f,*]

[a] São Paulo State University (Unesp), School of Pharmaceutical Sciences, Araraquara, São Paulo, Brazil
[b] São Paulo State University (Unesp), School of Agricultural and Veterinarian Sciences, Jaboticabal, São Paulo, Brazil
[c] São Paulo State University (Unesp), School of Technology and Sciences, Presidente Prudente, São Paulo, Brazil
[d] Centro de Bioinformática, Simulación y Modelado (CBSM), Universidad de Talca, Talca, Chile
[e] São Paulo State University (Unesp), Institute of Chemistry, Araraquara, São Paulo, Brazil
[f] São Paulo State University (Unesp), School of Sciences and Engineering, Tupã, São Paulo, Brazil

ARTICLE INFO

Keywords:
AMP
Chitosan
Enteric coating
HPMCAS
In vitro release
Microparticles

ABSTRACT

The incorrect use of conventional drugs for both prevention and control of intestinal infections has contributed to a significant spread of bacterial resistance. In this way, studies that promote their replacement are a priority. In the last decade, the use of antimicrobial peptides (AMP), especially Ctx(Ile^{21})-Ha AMP, has gained strength, demonstrating efficient antimicrobial activity (AA) against pathogens, including multidrug-resistant bacteria. However, gastrointestinal degradation does not allow its direct oral application. In this research, double-coating systems using alginate microparticles loaded with Ctx(Ile^{21})-Ha peptide were designed, and *in vitro* release assays simulating the gastrointestinal tract were evaluated. Also, the AA against *Salmonella* spp. and *Escherichia coli* was examined. The results showed the physicochemical stability of Ctx(Ile^{21})-Ha peptide in the system and its potent antimicrobial activity. In addition, the combination of HPMCAS and chitosan as a gastric protection system can be promising for peptide carriers or other low pH-sensitive molecules, adequately released in the intestine. In conclusion, the coated systems employed in this study can improve the formulation of new foods or biopharmaceutical products for specific application against intestinal pathogens in animal production or, possibly, in the near future, in human health.

1. Introduction

Intestinal infections caused by *Salmonella* are a major public health problem of global importance since their spread is quick and easy [1]. In addition, due to uncontrolled use of drugs, these bacteria are acquiring resistance against conventional antibiotics [2]. Therefore, there is an urgent need for new food additives with efficient antimicrobial activity that may replace these standard drugs [3].

Antimicrobial peptides (AMP) are molecules naturally produced by different living organisms and they have the ability to control and combat pathogenic bacterial and fungal microorganisms [4,5]. AMP can act by blocking intracellular targets or disturbing the lipids of the bacterial cell membrane, which destabilizes bacterial homeostasis and leads to cell lysis [6,7]. Some AMP molecules face a challenge posed by the

* Corresponding author. São Paulo State University (Unesp), School of Sciences and Engineering, Tupã, São Paulo, Brazil.
** Corresponding author. São Paulo State University (UNESP), School of Pharmaceutical Sciences, Araraquara, São Paulo, Brazil.
E-mail addresses: cesar.roque@unesp.br (C.A. Roque-Borda), eduardo.vicente@unesp.br (E.F. Vicente).
[1] We cite in memory of Ms. Anna Beatriz Toledo Borges, member of the Tuberculosis Research Laboratory and scientific initiation researcher of PIBIC-CNPq/Brazil.

https://doi.org/10.1016/j.biomaterials.2022.121978
Received 24 March 2022; Received in revised form 3 November 2022; Accepted 20 December 2022
Available online 22 December 2022

physical-chemical and structural instability in biological systems, since they can be degraded by proteolytic enzymes or hydrolyzed at acid pH [8]. In food technology, the microencapsulation method is useful for preserving sensitive and easily degradable bioactive compounds such as antioxidants, essential oils, and bioactive peptides [9].

In microencapsulation, sodium alginate is the most commonly used polymer, which is negatively charged (i.e., carboxylic acid). It performs an ion exchange with a polyvalent salt, usually Ca^{2+}, forming an "egg box" [10]. Also, alginate is one of the safest products used in the food industry [11]. Another widely used biopolymer is chitosan, which has efficient mucoadhesive properties, facilitating its application due to its excellent biocompatibility. Chitosan is biodegradable and can improve the drug release in the intestinal microbiota [12,13]. Previous studies revealed that this natural polymer can be used as an efficient layer of alginate-based microparticles loaded with antioxidants, which helped to keep the bioactive compound safer during its passage through the gastrointestinal tract [14]. Besides, a previous study showed that cellulose derivatives have protective properties to maintain the structure and activity of AMP stable when used as an enteric coating [15]. In this way, an alginate-based microparticle system, double-coated with hydroxypropylmethylcellulose acetate succinate (HPMCAS) and chitosan, may confer the protection and physicochemical stability necessary for the AMP and achieve bacterial control against *Salmonella* spp. in the intestinal tract [16]. In this study, the Ctx(Ile^{21})-Ha AMP was chosen because it has efficient properties against bacteria from the poultry and food sector [17] and has been extensively studied by our research group [18,19].

Therefore, to prevent intestinal infections, this work aimed to (i) microencapsulate Ctx(Ile^{21})-Ha AMP in cross-linked alginate and protect it with both HPMCAS and chitosan, (ii) evaluate its physicochemical parameters, (iii) study its release in a simulated and controlled gastrointestinal tract, and (iv) determine its antibacterial activity against pathogens, such as *Salmonella* spp. and *E. coli*.

2. Materials and methods

2.1. In silico studies

2.1.1. Characterization and analysis of Ctx(Ile^{21})-Ha AMP

Before any experimental procedure, it is worth taking advantage of the current *in silico* tools. Hence, the likelihood of bioactivity, physicochemical parameters, enzyme digestion and absorption, distribution, metabolism, excretion, and toxicology (ADMET) were predicted using several web servers to retrieve the desired information from the Ctx (Ile^{21})-Ha AMP. The following methodology was adapted from Fan et al. [20]. Moreover, a complementary structural bioinformatic analysis is included to explore the relevance in the receptor-peptide interaction at the atomistic level.

2.1.2. Secondary structure prediction of Ctx(Ile^{21})-Ha AMP

The secondary structure of Ctx(Ile^{21})-Ha AMP was modeled using the PEP-FOLD3 web server [21]. The structural criteria to select the best model were the energy score sOPEP from PEP-FOLD3 and the previous structural characterization of the peptide [17,18,22]. The visualization of the model results was performed using Visual Molecular Dynamics software [23].

2.1.3. Docking protein-peptide

Relevant receptors from bacteria that have available experimental structure were retrieved from the PDB database (http://www.rcsb.org) [24], and the pre-docking structures were prepared using the Dock Prep module [25,26] from UCSF Chimera software [27], deleting waters and molecules from the crystallographic process. Also, the secondary structure of the peptide was processed in the same way. The structures prepared from the receptors and the Ctx(Ile^{21})-Ha peptide model were tested through molecular docking assay. The software LightDock was used to perform protein-peptide docking [28–30]. LightDock uses the Glowworm Swarm Optimization algorithm in its docking protocol, to perform molecular docking of protein-protein, protein-peptide, and protein-DNA systems [31]. In each case of receptor-peptide docking, the parameters were set as 400 swarms, 200 glowworms, and 100 steps of simulation, as suggested by the authors, and the energy computation is based on DFIRE scoring function [32]. PLIP software was used to predict protein-peptide interactions. The visualization of molecular docking results was performed using the PyMOL Molecular Graphics System, Version 2.0 Schrödinger, LLC. was used to visualize [33].

2.1.4. Prediction of bioactive capacity, physicochemical features, and toxicity

The likelihood of bioactivity was predicted using the PeptideRanker web server [34]. The *N*-to-1 Neural Network method of PeptideRanker predicts the probability of a peptide being bioactive. In this sense, when PeptideRanker computes a score greater than 0.5, the peptides under study are considered bioactive. The physicochemical properties of Ctx (Ile^{21})-Ha AMP with the C-terminus amide group, i.e., molecular weight, extinction coefficient, iso-electric point, net charge (pH 7) and solubility, were analyzed using PepCalc (available at http://pepcalc.com/). This free software was developed by Innovagen AB, Lund, Sweden. Additionally, toxicity prediction was performed by the ToxinPred web server [35]. The algorithm combines the support vector machine and motif analysis to predict, with high accuracy, the toxicity of peptides with 35-mer or less.

2.1.5. Enzymatic digestion

The enzymatic process was simulated using PeptideCutter [36]. A probability threshold was set at 60%, simulating the cleavage with digestive enzymes chymotrypsin (Enzyme Commission number (EC): 3.4.21.1), trypsin (EC: 3.4.21.4), and pepsin (pH = 1.3 and > 2, EC: 3.4.23.1). In addition, the Proclave web server, which combines sequence and structural information to predict cleavage sites, was used with enzymes chymotrypsin (EC: 3.4.21.1), pepsin (EC: 3.4.23.1), and elastase II (EC: 3.4.21.71) [37].

2.1.6. ADMET analysis

The one-letter code sequence of Ctx(Ile^{21})-Ha peptide was converted into a simplified molecular input line entry system (SMILES) string format, using the PepSMI online tool (developed by NovoPro Bioscience Inc. And available at https://www.novoprolabs.com/tools/convert-peptide-to-smiles-string), modified to present the C-terminus amide group and visually inspected with the Smi2Depict online tool (available at http://cdb.ics.uci.edu/cgibin/Smi2DepictWeb.py#). Then, the SMILES string was used in ADMET lab 2.0 web server to predict the following features: absorption (human intestinal absorption, human oral bioavailability, Caco-2 permeability), distribution (plasma protein binding, P-glycoprotein [P-gp] substrate and inhibitor, blood-brain barrier penetration), metabolism (Cytochrome P450 [CYP450] substrate inhibitor, pharmacokinetics transporters), excretion (half time, renal clearance), and toxicity [38].

2.2. Production of samples

2.2.1. Synthesis, purification, and characterization of the Ctx(Ile^{21})-Ha antimicrobial peptide

The Ctx(Ile^{21})-Ha antimicrobial peptide (hereafter Ctx) was manually synthesized by Fmoc-SPPS method, characterized, and purified (see the complete procedure in Roque-Borda et al. [15]).

2.2.2. Production of coated microparticles

To obtain the microparticles, a dispersant solution (DS) containing 2% sodium alginate solubilized at 100 rpm at RT overnight, to avoid the presence of suspended particles, and another crosslinking solution (RS) with 5% aluminum chloride were used. Ctx(Ile^{21})-Ha antimicrobial

peptide (1 mg/mL) was added to the DS, previously solubilized with 500 μL of ultrapure water. The microparticles were obtained according to Anbinder et al. [14]. Briefly, a hypodermic syringe (0.8 mm × 40 mm, G21 needle) was loaded with DS and dripped manually in RS using a shaker at 100 rpm at RT. The resulting microparticles were transferred to 0.2 mol/L acetic/acetate buffer, pH 5.5, to remove excess aluminum ions, and then filtered. They were divided into two coating systems using hypromellose acetate/succinate powder (HPMCAS-LF, AQOAT® - Grade AS-LF; Shin-Etsu Chemical Co., Ltd.) and commercial chitosan (20.31% degree of deacetylation, calculated by FTIR; see Supplementary Material).

2.2.2.1. HPMCAS-system (HPMCAS). The alginate-based microparticles obtained were suspended in coating solution 1 (CS1) for 30 min at 50 rpm at RT. CS1 was prepared with 10% (w/w) HPMCAS, 75.2% (w/w) ethanol, and 18.8% water.

2.2.2.2. Chitosan-system (CHIT). The alginate-based microparticles obtained were suspended in coating solution 2 (CS2) for 30 min at 50 rpm at RT. CS2 was prepared by pouring 1% chitosan into 20 mL of 1% acetic acid.

2.2.2.3. Chitosan/HPMCAS-system (CHIT/HPMCAS). The microparticles obtained were suspended in a (1:1 CS1/CS2) bilayer coating for 30 min at 50 rpm at RT.

2.3. Characterization of microparticles

2.3.1. Loading efficiency

The loading efficiency was based on a previously published methodology [39]. Briefly, a 5% sodium citrate solution was prepared to remove the alginate from the capsules for 2 h at RT under horizontal shaking. Subsequently, Ctx was extracted with (1:1, v/v) A/B at 3600 × *g* for 10 min at RT. The procedures were performed in triplicate. The calculations were performed based on the UV absorbances at 280 nm obtained in a UV/VIS spectrophotometer (Shimadzu UV1800, Japan), using Lambert-Beer equation (Equation (1)) [40]:

$$Abs = c\ x \diagup x\ \varepsilon \tag{1}$$

where *Abs* is the obtained UV absorption (arbitrary units), *c* is the concentration, ⁄ is the quartz cuvette diameter, and ε the molar absorptivity. Then, the peptide was rapidly extracted with solvents A and B for 2 h and centrifuged. For the analysis, 1 mL of solution was read at 280 nm in the spectrophotometer and calculated using as a parameter the tryptophan absorption in the following wavelength: ε, molar absorptivity, of 5690 M^{-1} cm^{-1}. The encapsulation efficiency (EE) was calculated using Equation (2), with 1 mL of the previously prepared solution:

$$Encapsulation\ efficiency\ (EE\ \%) = \frac{TP - FPC}{TP}\ X\ 100 \tag{2}$$

where *TP* is the total Ctx peptide content supplied and *FPC* is the free peptide content of the microcapsules.

2.3.2. Morphological analysis

The internal structure of the microparticles was evaluated using a SEM scanning electron microscope (JSM 6610 LV, USA). The microparticles were sealed with gold and photomicrographs were taken up to 15,000 × magnification. The samples were analyzed under 2.0 kV energy emission current of 10 μA, a current probe of 9, and a work distance of 6.5 mm. The size of the microparticles was obtained using the free software Image J 1.53K Java 1.8.0_172, from the National Institute of Health, USA.

2.3.3. Fourier-transformed infrared (FTIR) analysis

FTIR spectra were obtained using a spectrometer (PerkinElmer, Frontier model, USA) with attenuated total reflectance (ATR). Peaks and bands were expressed in transmittance with a scan of 4000 to 400 cm^{-1}, and resolution of 4 cm^{-1}. Spectra were analyzed using OriginPro 2019 software.

2.3.4. Thermal analysis

To understand the thermal behavior of the microparticles loaded with the Ctx(Ile^{21})-Ha antimicrobial peptide, differential scanning calorimetry (DSC) and thermogravimetry (TGA) and their first derivative (DTG) analyses were used. The selected temperature range was 30°C-600 °C, using DSC-TGA Equipment (SDT Q600 V20.9 Build 20, TA Instruments). A mass of 10 mg of microparticles was analyzed at a heating rate of 5 °C min^{-1}, wrapped in a platinum cell, and kept under a synthetic air atmosphere.

2.3.5. X-ray diffraction analysis

The crystallographic studies were performed using an X-ray diffractometer (XRD-6000, Shimadzu) at 40 kV and 30 mA, CuKα1 (λ = 1.5406 Å) and CuKα2 (λ = 1.5444 Å) radiation, at 2° min^{-1} (angular velocity) from 10° to 80° (2θ). The microparticles were placed on glass support without fixative. Method one was used to determine the Crystallization Index (CrI) according to Park et al. [41]. This index was calculated for the samples using Equation (3), as previously reported [42,43]:

$$CrI = \frac{I_{002} - I_{am}}{I_{002}}\ X\ 100 \tag{3}$$

where I_{002} is the intensity around 22.5° (crystalline domain) and I_{am} is the intensity around 18° (amorphous domain).

2.4. In vitro studies

2.4.1. Antimicrobial activity of Ctx(Ile^{21})-Ha AMP

Antimicrobial activity (AA) was tested in five bacteria of importance in food safety and health, provided by the Ornithopathology Laboratory of the Department of Pathology, Theriogenology, and One Health, of São Paulo State University (Unesp), School of Agricultural and Veterinarian Sciences, Jaboticabal. The pathogenic bacteria tested were *Salmonella* Typhimurium (F98), *Salmonella* Enteritidis (P125109), *Salmonella* Heidelberg, *Salmonella* Infantis (isolated from symptomatic chickens), and *Escherichia coli* (ATCC 25922). All bacteria were cryopreserved in 30% glycerol at −80 °C.

Minimal Inhibitory Concentration (MIC) of the Ctx(Ile^{21})-Ha peptide against strains was determined after 24 h of incubation at 37 °C, using the microdilution method, according to the requirements of the M100 manual [44]. Previously, bacterial strains were grown in Luria-Bertani broth (LB) (Oxoid, United Kingdom) for 24 h at 37 °C for adaptation. Then, bacterial cultures were adjusted to 0.5 McFarland turbidity standard and placed on 96-well plates at seven different concentrations (2–128 μg/mL) of the peptide in Mueller-Hinton broth (MH) (Oxoid, United Kingdom). The growth kinetics was determined after 24 and 72 h.

2.4.2. In vitro release profile

The gastrointestinal tract (GIT) was mimicked by immersing 50 mg of microparticles in 10 mL of the simulated gastric fluid (SGF) solution and the same proportions in the simulated intestinal fluid (SIF) solution. The SGF was prepared using a 0.1 mol/L HCl solution at pH ≈ 2. The SIF was prepared using Buffer Sorensen's phosphate at a final pH of 7.4 [14]. The sampling was carried out at different times (5, 10, 20, 40, 60, 120, and/or 180 min) and quantified by Equation (1) at 280 nm.

The mechanisms involved in the drug release process were evaluated through the release data obtained, which were treated with different mathematical models (Baker - Londsdale, First-Order, Higuchi, Hixson - Crowell, Korsmeyer-Peppas, and Weibull). The Korsmeyer-Peppas and

Weibull models were applied using release data of up to 60% and 62.3%, respectively.

2.4.3. In vitro enzymatic inhibition

For enzymatic digestion, the protocol previously published by Meneguin et al. [45] was employed. Briefly, 5 mg/mL of microparticles with different coatings were placed in a SGF solution with 0.3 mg/L of pepsin and in a SIF solution with 3.2 mg/mL of pancreatin. The sampling was carried out at different times and quantified by Equation (1) at 280 nm. An identical solution without microparticles was used as a blank for quantification readings.

2.5. Cytotoxic activity

For the cytotoxic activity, Caco-2 cells (immortalized human colorectal adenocarcinoma cells) were used as a model of the intestinal barrier [46]. Caco-2 cells were thawed and used after 8 passages, cultured in Dulbecco's Modified Eagle's Medium - High Glucose (DMEM-HG). Caco-2 cells were seeded at a density of 1.5×10^4 cells/-well in 96-well microplates at different concentrations (2–0.0625 mg mL^{-1}) of the analyzed double-coated microparticles for 24 h in DMSO (10% v/v). Pure peptide was used as a positive control and DMEM-HG as a negative control. The samples were quantified by applying a volume of 30 μL of resazurin 0.01% and read after 24 h at 530/590 nm.

2.6. Statistical analyses

All experiments were done in triplicate and statistical analyses data were performed using the software GraphPad Prism, version 8.2.1. Tukey's test was used to compare the means when the overall *P*-value of the experiment was below the value of significance ($P < 0.05$). The Sigma Plot 11.0 software was employed for the mathematical of prediction of the drug release kinetics.

3. Results and discussion

3.1. In silico results

3.1.1. Ctx(Ile^{21})-Ha AMP has a potential bioactive capacity

The Ctx(Ile^{21})-Ha AMP (Ctx) presents a molecular weight of 2289.72 g/mol, an extinction coefficient of 5690 M^{-1} cm^{-1}, net charge of +4.00 (pH = 7) and is poorly hydrophilic, with a – 0.20 value (Table S2 and Figure S1). In addition, it was subjected to PeptideRanker analysis to predict the probability of being a potential bioactive peptide. The algorithm has only an 11% false-positive rate for long peptides (greater than or equal to 21 amino acids long) [34], predicting for Ctx 97% probability of being a bioactive peptide (Table S1) [18,19,47]. Moreover, it is interesting to note that the toxicity analysis, using the support vector machine approach, revealed that Ctx does not belong to the toxin group database, given that ToxinPred was trained with allergenic and toxin peptides [35]. According to Ferreira Cespedes et al. [17], Ctx exhibited high hemolytic activity and, in agreement with previous studies, Roque-Borda [15] indicated that encapsulated AMP in polymeric microstructures could efficiently overcome this problem, since the Ctx peptide microcapsules lost their hemolytic activity and enhanced their antimicrobial activity.

3.1.2. Structural models and docking receptor-peptide

The resulting models from the PEP-FOLD3 are displayed in Figure S1. The prediction of noncovalent interaction analysis for the PDB structure is shown in Data S1, and molecular docking results are displayed in Table S1. In this research, some relevant receptors that have an experimentally solved structure in the PDB underwent the above-mentioned protocol to investigate the affinity of the peptide to a bacterial protein, as previously suggested. In Table S1, the peptide displayed a favorable energy score to interact with all receptors, *i.e.*, the energy of the protein-peptide complex is negative (from −22.05 to −59.41 kcal/mol). The score calculated by the DFIRE function has a strong correlation between theoretical and experimental binding affinities in its implementation, suggesting an interesting likelihood of protein-peptide interaction [48]. Moreover, in almost all cases, the peptide interacts deeply with its receptor (Fig. 1), burying itself inside the protein structure. The multidrug resistance regulator RamR from *Salmonella* Typhimurium (PDB ID 6IE8) is the exception to the phenomenon, although the energy of the complex is favorable. Furthermore, Fig. 1 shows that peptide is deep inside the structure of receptors, and the most frequent interactions are the hydrophobic interaction and hydrogen bonds (Supplementary data 1). However, the carboxylate group of the peptides ASP-1, ARG-37, and ARG-56 from LT2 neuraminidase of *Salmonella* Typhimurium (PDB ID 2SIL) exhibits a salt bridge interaction, which could explain the affinity increment between them, compared to other cases (Table S1). It should be highlighted that these residues (ARG-37 and ARG-56) belong to the active site [49].

These results demonstrate and corroborate that the peptide has an interaction with the receptors of the bacteria under study, which makes the peptide promising against these intestinal pathogens, including multidrug-resistant bacteria such as the one previously described. The results show similarity to the results obtained with protein receptors (PDB ID 3L9V, 1QJ8, 6IE8, 2SIL, 3T88, and 1HNJ) analyzed in other studies [50–54].

3.1.2.1. Ctx(Ile^{21})-Ha AMP is vulnerable to enzymatic digestion. Enzymatic digestion was predicted for the Ctx peptide using enzymes from the stomach (pepsin) and intestine (chymotrypsin, trypsin, and elastase) *in silico*, using two different programs (Table 1). For the enzymatic simulation using PeptideCutter, pepsin revealed more than 60% probability of cleavages at amino acid residues in positions 2, 3, 14, and 19 (pH = 1.3). Meanwhile, at pH ≥ 2, the cleavage sites were 1, 2, 3, 14, and 19 (Table 1). On the other hand, the Proclave approach predicted pepsin cleavages at 4, 10, 11, 12, 13, 14, and 15 residue positions (Table 1).

In addition, pancreatic enzymes chymotrypsin, trypsin, and elastase II were used to simulate peptide digestion. Chymotrypsin can cleave the Ctx peptide in sites 2 and 14 (Table 1), with 87.1% and 71.3% probability, respectively, according to the PeptideCutter algorithm, whereas Proclave program predicted 14 and 15-mer as cleavage sites (Table 1). Ctx peptide underwent *in silico* trypsin digestion with PeptideCutter software, presenting cleavage sites at 7, 8, 11, and 18 positions, with 90.5%, 61.9%, 100%, and 88.4% probability, respectively. Moreover, using Proclave software, elastase II predicted sites at 12, 16, and 17-mer. Hence, *in silico* predictions suggest that Ctx will be digested in the digestive system, demanding previous strategy/protection to prevent peptide degradation.

3.1.3. ADMET analysis

SMILES format for Ctx peptide was achieved (Table S3), and the most relevant data in drug design are discussed. Table S4 shows the complete and detailed study.

During absorption, the Ctx peptide resulted in low active permeability in Caco-2 cells. However, a previous study demonstrated the intestinal cell barrier permeability of Ctx using alginate microparticles coated with HPMCAS, since the biopolymers in the formulation can help to open the intestinal barrier [16]. Likewise, high passive permeability was observed in the Madin-Darby canine kidney (MDCK) cell, which would be related to the output parameters of the drugs and the active transport given by the P-gp; and the power to cross the blood-brain barrier (BBB) was also predicted [55]. Finally, another relevant parameter was its potential use against P-gp efflux pumps, which is an important feature to be evaluated, since bacterial resistance is currently a WHO priority [2].

Ctx(Ile^{21})-Ha peptide distribution studies indicated 30.87% plasma

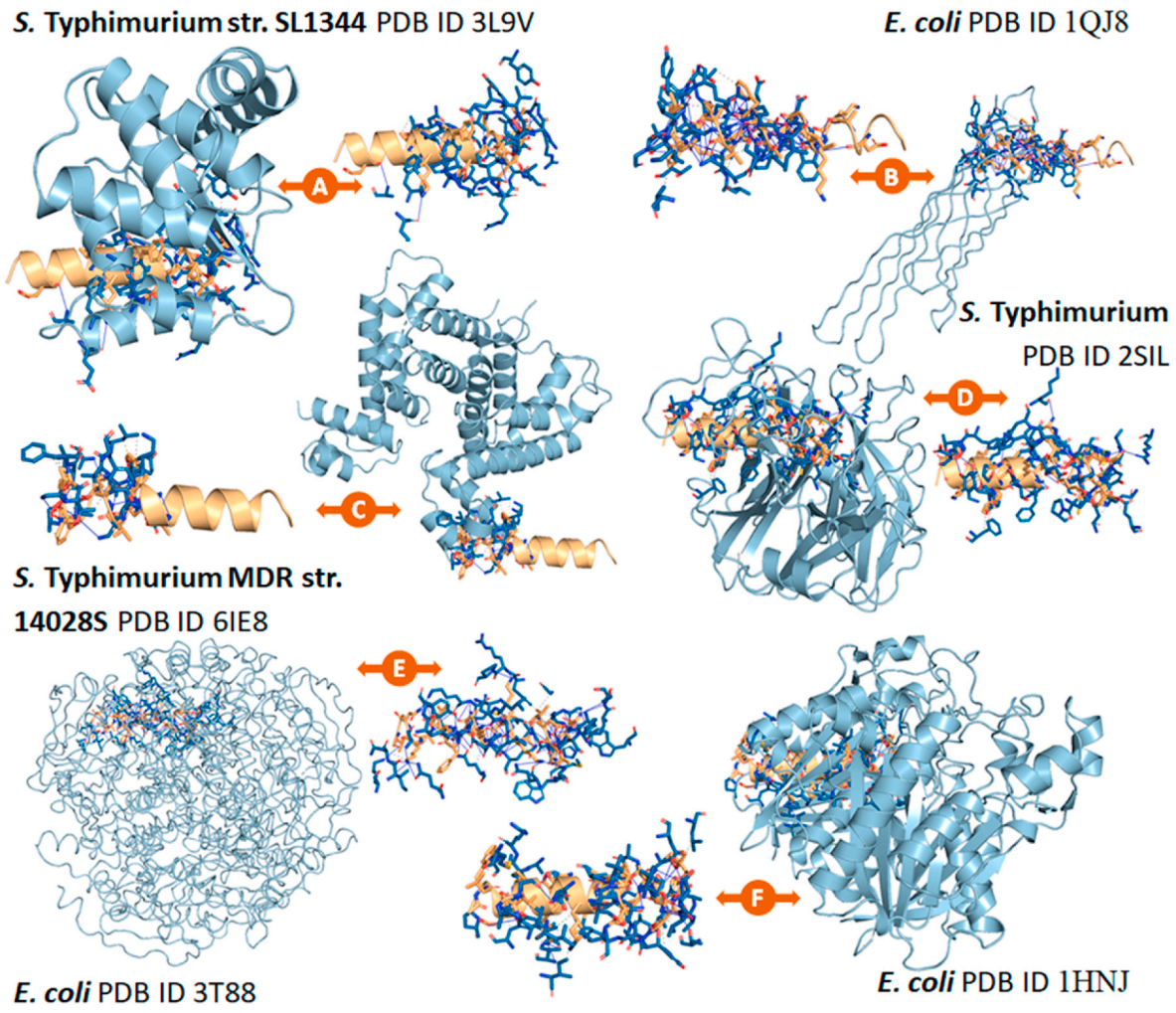

Fig. 1. Visualization of docking results and protein-peptide (Ctx-bacteria) interaction. The position with the most negative score of LightDock and the zoom showing the interactions are displayed. Receptors are colored in metallic cyan and, from top to bottom, present the PDB ID **(A)** 3L9V, **(B)** 1QJ8, **(C)** 6IE8, **(D)** 2SIL, **(E)** 3T88, and **(F)** 1HNJ. Ctx peptide is displayed in metallic orange. Hydrophobic interaction, hydrogen bonds, and salt bridge are represented in gray, blue, and yellow lines, respectively. (For interpretation of the references to color in this figure legend, the reader is referred to the Web version of this article.)

Table 1
Simulation of enzymatic digestion on SGF. Enzymatic cleavage was performed by PeptideCutter and Proclave web servers. The "||" symbol represents the cleavage site. Only Proclave results are shown with a score greater than or equal to 0.1. The complete set of Proclave results is presented in Table S2.

Enzyme	EC number	Cleavage Site	Software
Pepsin (pH = **1.3**)	3.4.23.1	GW||L||DVAKKIGKAAF||NVAKN||FI	PC
Pepsin (pH > **2**)	3.4.23.1	G||W||L||DVAKKIGKAAF||NVAKN||FI	PC
Pepsin (pH > **7.2**)	3.4.23.1	GWLD||VAKKIG||K||A||A||F||N||VAKNFI	Pr
Chymotrypsin (pH > **7.2**)	3.4.21.1	GW||LDVAKKIGKAAF||NVAKNFI	PC
Chymotrypsin (pH > **7.2**)	3.4.21.1	GWLDVAKKIGKAAF||N||VAKNFI	Pr
Trypsin (pH > **7.2**)	3.4.21.4	GWLDVAK||K||IGK||AAFNVAK||NFI	PC
Elastase II (pH > **7.2**)	3.4.21.71	GWLDVAKKIGKA||AFNV||A||KNFI	Pr

*PC = PeptideCutter; Pr = Proclave.

protein binding, probability of being BBB+, optimal distribution volumes (0.364 L/kg), and 28.66% for the fraction unbound in plasms, the last two being the key parameters of pharmacokinetics and drug discovery [56]. The results of the metabolic study indicated that the Ctx peptide is not a substrate; nor does it induce the expression of CYP1A2. However, there is 0.3% probability indicating its inhibition. Inhibition of the CYP1A2 enzyme is evaluated to identify non-carcinogenic drugs, i.e., it does not cause cancer, but an enzymatic action could transform the substance into a carcinogenic molecule [57]. Finally, Ctx peptide also had no effect on the expression of CYP2C19 and CYP2C19, which would be involved in the accelerated degradation of the bioactive substance or develop genetic polymorphisms [58,59].

Excretion studies showed that the Ctx peptide has a long half-life, which indicates that with controlled use at adequate doses, the molecule can be properly excreted. For this reason, microencapsulation could control the release of the Ctx peptide, as proposed elsewhere [60]. Ctx peptide toxicity showed 0.3% and 11.3% of the Ames test (for mutagenicity) and rat oral acute toxicity, respectively. Also, the results showed 0.1% probability of drug-induced liver injury (no risk) and herG blocks (inactive). Therefore, the low toxicity found and, consequently, the few adverse effects, led to a complete study, both *in vitro* [15] and *in vivo* [47] strategies, with different biotechnological applications.

3.2. Characterization of samples

3.2.1. Peptide purification and characterization

Purification procedures and characterization by HPLC and mass spectrometry, respectively, of the Ctx(Ile^{21})-Ha peptide were previously reported by our research group, with more than 95% purity degree [15].

3.2.2. Characterization of microparticles

The EE% of alginate-based microparticles from ionic gelation (named C + Ct) was 84.52%, similar to those previously reported [15]. This high EE value indicates the possibility of an attraction between the anionic alginate ions and the cationic Ctx peptide [61].

3.2.3. Morphological results

The micromorphology of the coated microparticles favored internal conformational differentiation (Fig. 2). It was possible to observe different ordering between the microparticles of the CHIT/HPMCAS system, in comparison with other samples, which corroborates the FTIR results obtained, by means of electrostatic attraction during the coating process [14]. The first studies on the interaction of encapsulation with polycations demonstrated the great affinity that alginate has for certain compounds, such as poly-L-lysine and chitosan, which helps to strongly protect the active compound [62]. The microparticles used as control (without peptide/non-loaded) were named BR. Interestingly, as shown in Fig. 2, the CHIT/HPMCAS system exhibited a significant decrease in size (diameter and area), leading to a more compact capsule, based on its electrostatic force due to the ionic multilayer, as previously explained in layer-by-layer nanofibers [63].

3.2.4. FTIR results

All FTIR-spectra collected (Fig. 3) peaked at 1600 cm^{-1}, representing the alginate carboxyl groups, which are present in all microparticles [64]. The amide I band is an important feature within the structure of all proteins and peptides, and it was confirmed at 1260 cm^{-1} [65]. Ctx (Ile^{21})-Ha peptide-spectrum (pure) was previously reported and used as a reference [15]. In all the coating systems, a peak at 2930 cm^{-1} was shown, which reveals stretching vibrations of the C–H group [64].

CHIT-coated system showed a strong binding between the chitosan NH_2 groups and alginate, forming a chitosan-amide II band, a peak evidenced at ~1550 cm^{-1} [14]. HPMCAS-coated system exhibited characteristic acetate/succinate bands at ~1400 cm^{-1}, which allows the study of the possible interactions of its side chains with other polymers [66]. The presence of carbonyl groups from all samples was indicated at 1740 cm^{-1}, and this band was modified when the system coated with CHIT/HPMCAS was obtained, showing a molecular interaction between the monolayer microparticles and the HPMCAS coating solution [67]. The CHIT/HPMCAS system showed a decreased intensity in this band, as an electrostatic interaction was obtained between anions (acetate/-succinate) and cations (chitosan), which allowed a firm increase in the protective coating barrier, in agreement with Nunthanid et al. [68].

3.2.5. Thermal results

The thermograms of Ctx pure peptide indicate that the molecule exhibited thermostability up to ~70 °C, as previously reported [15]. However, the use of polymers to obtain microparticles can influence the loss of mass at high temperatures, and this is due to greater intramolecular collision of each of them [69]. DTG (first derivative of TGA) indicates the relevant mass loss events, and in all samples, these events were similar. Therefore, no thermal instability between Ctx and alginate was observed in the assays.

The alginate microparticles (BR and C + Ct, Fig. 4) displayed characteristic endothermic events, such as the loss of water and fusion of the polycation-polymer complex resulting from cross-linking with Ca^{+2} ions at 95 °C and 184 °C, respectively [70]. An exothermic event was also recorded at 360 °C, presumably caused by the "egg box" formation [71]. According to Hosseini et al. [71], cationic AMP, such as nisin, can perform electrostatic interaction with anionic polymers. This situation can corroborate our findings, where Ctx (net charge of +4 at physiological pH) and alginate (negatively charged) can interlace stably. Further evidence is offered by the decrease in the endothermic event at

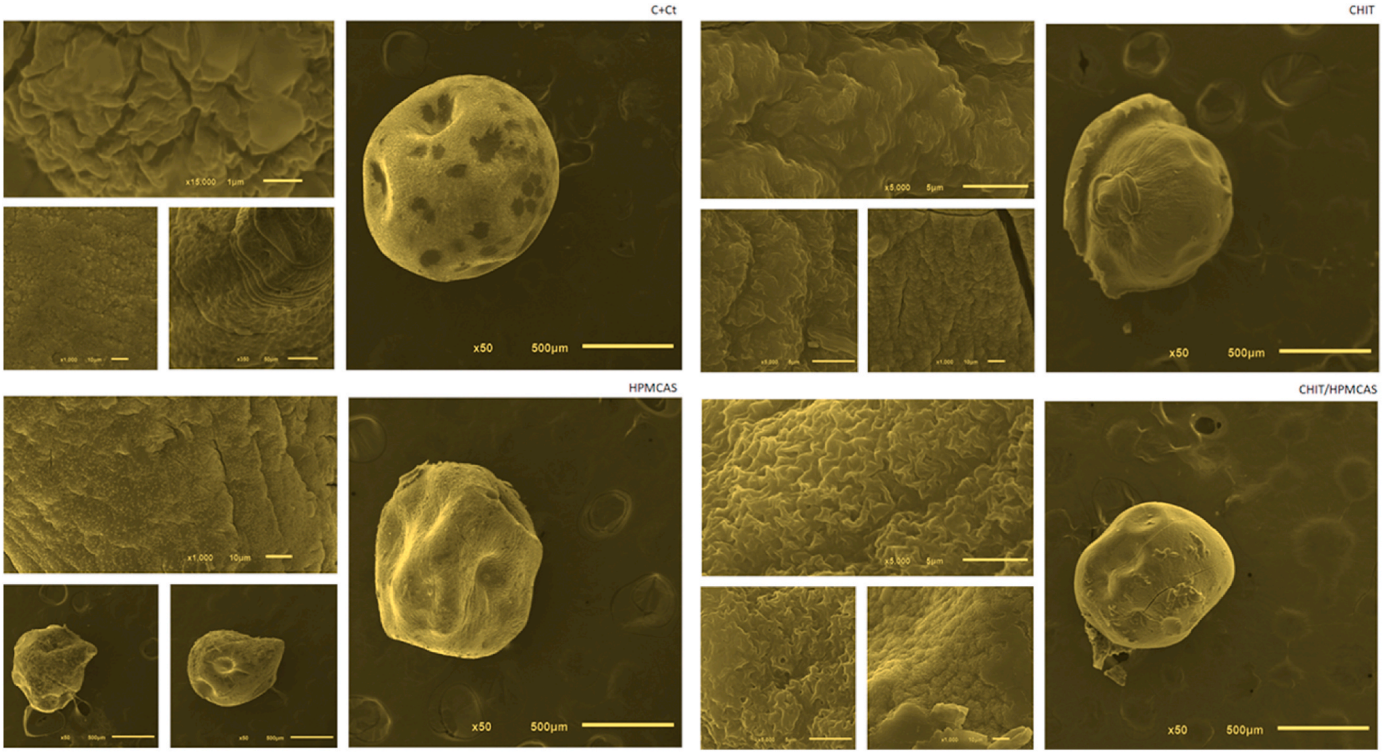

Fig. 2. Photomicrographs of the Ctx peptide-loaded microparticles. The results obtained by analysis in ImageJ software showed diameter values of 1121.22 ± 98.57^{a}; 1013.6 ± 87.35^{a}, 998.64 ± 25.23^{a}; and 840.09 ± 17.39^{b} µm for C + Ct, CHIT, HPMCAS, and CHIT/HPMCAS, respectively.

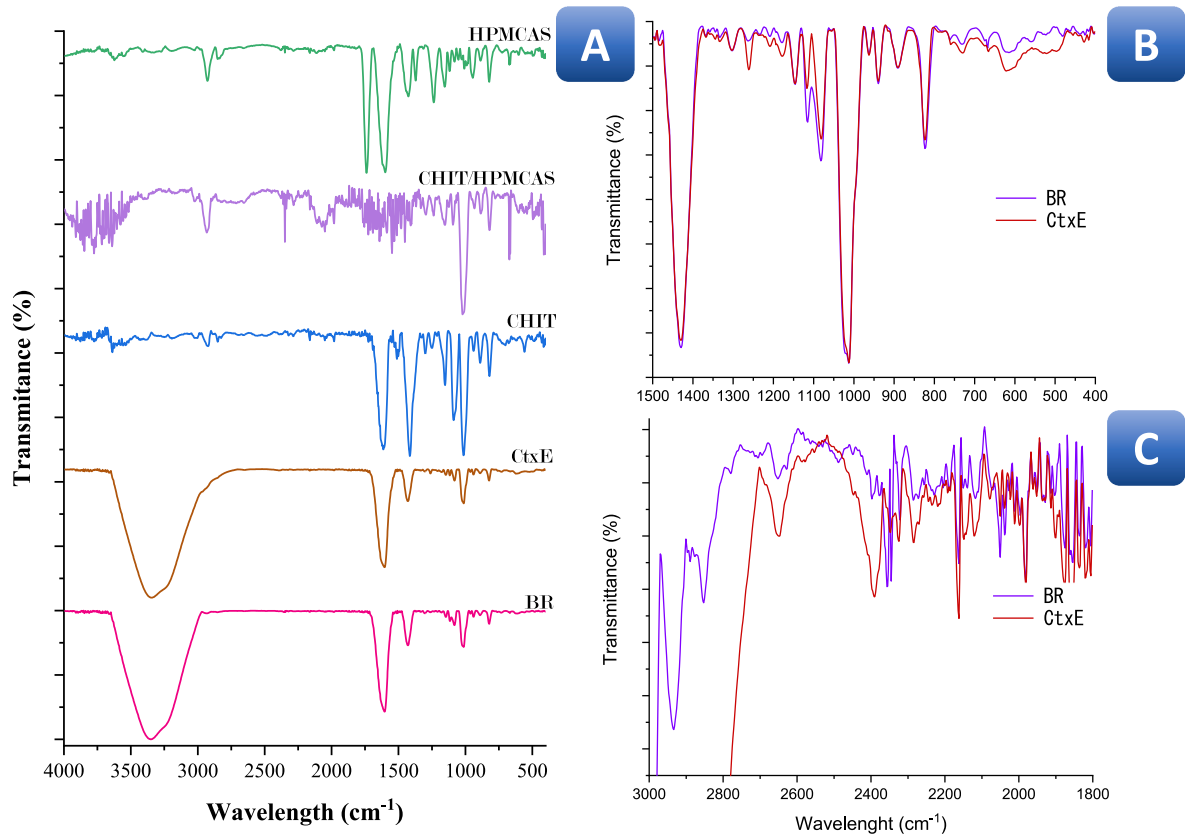

Fig. 3. A. FTIR-spectra from alginate-based microparticles in different coated systems. The alginate capsules without Ctx peptide were identified as BR to evaluate the differences between the incorporated peptide and the peptide subsequently coated with the different systems. **B.** FTIR spectrum from 1500 to 400 to visualize the modifications when the peptide is incorporated and **C.** FTIR spectrum from 3000 to 1800 to visualize the modifications when the peptide is incorporated.

70 °C, compared to BR and C + Ct. In the same way, the electrostatic interactions between all the coating systems studied show that all these events do not harm the application of Ctx(Ile^{21})-Ha AMP in this formulation, since its employment is carried out at RT. It was previously reported that the application of hydroxypropylmethylcellulose phthalate (HPMCP)-coated microparticles against *Salmonella* Enteritidis in laying hens resulted in a significant decrease in the mortality rates of infected chicks and led to weight gain, in addition to the existence of strong resistance and thermal stability, since the chicken coops stored the feed at 40 °C [47].

In summary, the TGA characteristics of the microparticles loaded with the Ctx peptide and coated with chitosan and HPMCAS were not modified. However, the CHIT/HPMCAS system presented a Tg-variance in its DSC-spectrum, resulting from ionic interaction.

3.2.6. *Crystallographic results*

Fig. 5 shows the X-ray diffraction patterns of all the analyzed samples. It is possible to observe that both microcapsules, with/without the Ctx peptide, exhibited an amorphous structure, which indicates their easy dissolution in aqueous media. Amorphous solids are more soluble than crystalline substances because of the low free energy in their dissolution [72]. According to Wang et al. [73], in the 20°–25° region, there is an increase in the intensity values, which may be related to the formation of small crystalline structures, probably due to metal ions giving rise to favorable cross-linking ("egg box" formation) when sodium alginate is exchanged with aluminum chloride [74]. The CHIT system exhibited two characteristic bands of its amorphous region, located at 15° and 22.5° [42,75], which is in good agreement with Nunthanid et al. [76]. Similarly, the HPMCAS crystalline structure was totally amorphous. However, in its enteric coating phase, it is possible to identify a band at 21.5°, which indicates the presence of the crystalline structure of cellulose I [43,64].

As it was prepared in an ethanolic solution, the HPMCAS system has a slight alkaline charge, which, when in contact with the positively charged chitosan, formed a pole attraction and optimized the coating process [61]. The CHIT/HPMCAS system allowed the reduction of the 15° and 22.5° bands, which consequently increased the stability of AMP in the biopharmaceutical formulation (alginate/chitosan/HPMCAS, strong disorganization of the semi-crystalline structure), increasing its bioavailability [75]. Furthermore, Table 2 shows CrI, and it is remarkably clear that there was no crystallization in BR, since this phenomenon was a feature of most drugs studied [77].

Molecular interaction is evidenced by the values of the crystallinity index, showing a significant difference from the developed systems. The CHIT system showed a high CrI, which means an increase in tensile strength. The alginate microparticles did not exhibit CrI and, as the Ctx peptide was added, there was a slight increase in this parameter. However, there was molecular interaction between chitosan and HPMCAS when the bilayer was made, since the CHIT/HPMCAS system CrI was low (from 41.07 to 26.79), which is a non-significant value in comparison with the HPMCAS system. HPMCAS, as a cellulose derivative, exhibited crystallinity properties (texture) [41].

3.3. *Antibacterial activity results*

The antibacterial activity results showed high MICs from Ctx(Ile^{21})-Ha antimicrobial peptide against the intestinal tract pathogens tested, such as *Salmonella* serovars and *E. coli* (Table 3) [44]. However, previous studies demonstrated that Ctx(Ile^{21})-Ha has higher AA against MDR bacteria, such as *Staphylococcus aureus*, *Pseudomonas aeruginosa* and *Acinetobacter baumannii* [15], and opportunistic fungi such as *Candida albicans* and *Cryptococcus neoformans* [18].

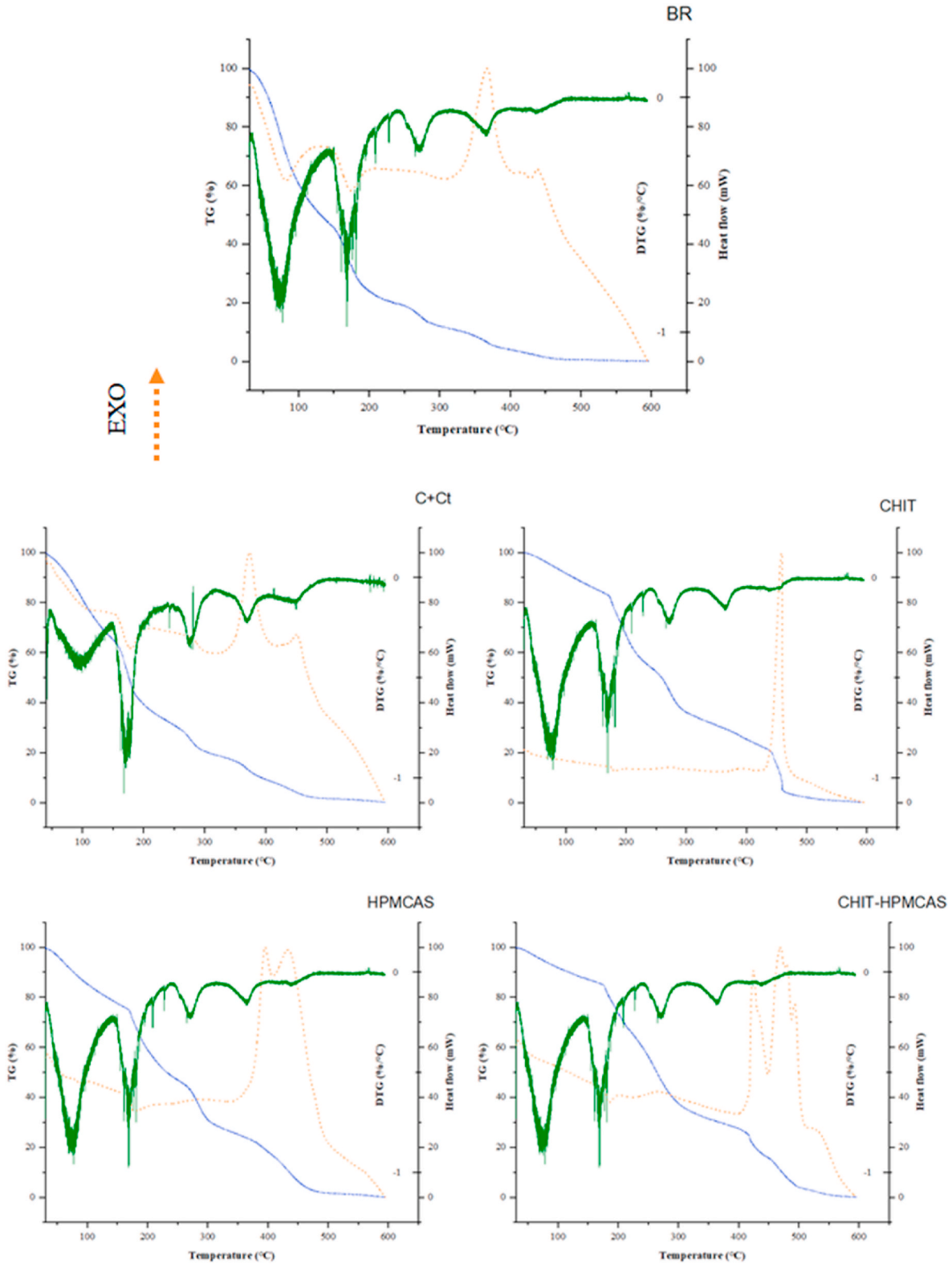

Fig. 4. Thermograms of the different stages of microencapsulation and coating.

Therefore, despite the higher MIC values presented by Ctx(Ile^{21})-Ha antimicrobial peptide against *Salmonella* serovars when compared to *E. coli* MIC values, this peptide can be a good option to prevent Enterobacteriaceae pathogens, especially as an alternative to the antimicrobials with growth promoters used in animals. The replacement of antimicrobials with peptides such as Ctx(Ile^{21})-Ha can reduce the consumption of these drugs, whose projections grow on an exponential scale [78]. The off-label use of antimicrobials is one of the biggest concerns of authorities in the animal production systems, as they have shown an enormous increase in resistant Enterobacteriaceae in a short period of time [79].

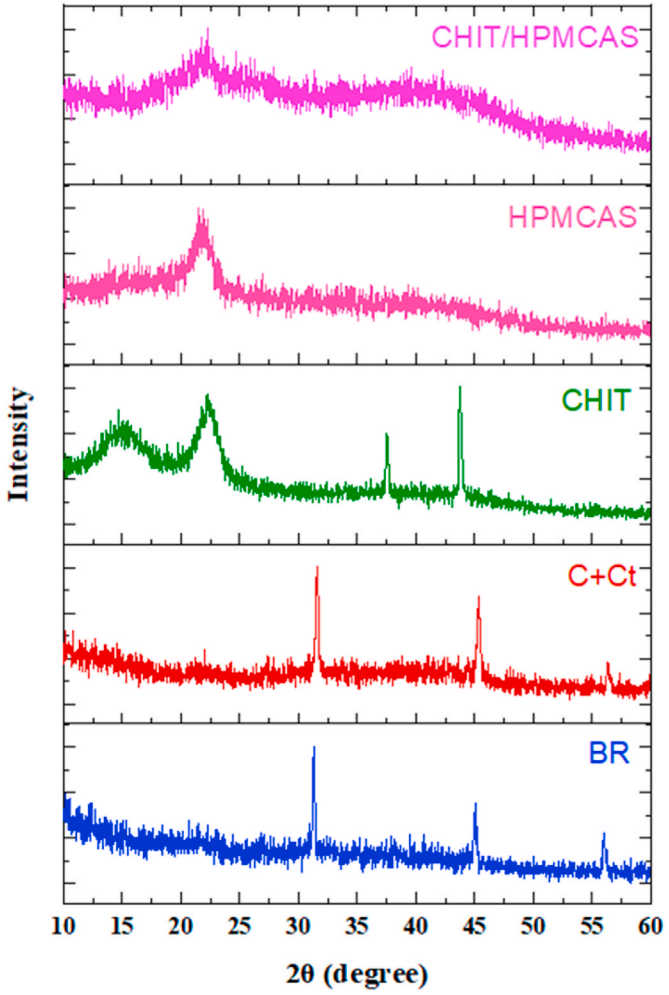

Fig. 5. X-ray diffractogram of the different stages of microencapsulation and coating.

Table 2
CrI of alginate-based microparticles by different coated systems. The CrI increased as bioactive compounds were incorporated. The entrapment of Ctx in the alginate capsules yielded semi-morpho results, as expected for the double- and single-coated systems using HPMCAS and chitosan.

Microparticle systems	Intensity (AU)		CrI[a]
	22.5°	18°	
BR	0.2712	0.2712	0.00[a]
C + Ct	0.1846	0.1692	8.34[b]
CHIT	0.8421	0.4962	41.07[c]
HPMCAS	0.6933	0.5200	25.00[d]
CHIT/HPMCAS	0.6588	0.4824	26.79[d]

[a] CrI = Crystallization Index. Note: Tukey's test (significant difference between means of CrI). Equal letters mean that there is no significant difference.

3.4. Simulated fluid results

In vitro peptide release was monitored under gastrointestinal conditions and the peptide release profile was analyzed for confirmation by LC/MS (Fig. 6). The CHIT system (Fig. 6) showed a maximum SGF release of 20.17 ± 3.86%, reflecting a slight escape of the peptide under acidic conditions. This can be explained by the high solubility displayed by chitosan under these conditions [80]. However, the ionic relationship between alginate and chitosan allowed chitosan to strengthen its coverage and avoid its rapid dissolution, in agreement with Anbinder et al. [14]. When compared with the HPMCAS system under the same conditions, a maximum release of 15.88 ± 4.86% was obtained, which means that optimization is still necessary, since the main objective of the formulation system is to fully protect the AMP and thus mitigate the loss of peptide. Some studies have reported that the release is highly dependent on the coating method [81–83].

Table 3
Minimal inhibitory concentration of Ctx(Ile^{21})-Ha peptide against *Enterobacteriaceae* strains in simulated gastric fluid. The Ctx(Ile^{21})-Ha peptide was evaluated at concentrations between 2 and 128 μg/mL.

Minimal inhibitory concentration (MIC)					
Bacteria[a]	STM	SE	SI	SH	EC
μg/mL	128.0	64.0	64.0	64.0	16.0
μM	111.8	55.9	55.9	55.9	14.0

[a] STM = *Salmonella* Typhimurium; SE = *Salmonella* Enteritidis; SI = *Salmonella* Infantis; SH = *Salmonella* Heidelberg; EC = *Escherichia coli*.

The use of HPMCAS in drug delivery formulations would improve the protection of bioactive compounds when they are placed as enteric coatings to prevent eruption or unexpected releases, due to different mechanical events within the GIT transport [84,85]. Likewise, its use is advantageous due to the content of carboxylic radicals, since they are capable of inactivating certain proteases that could denature the peptide in the intestine during the release [86]. Together, all these properties combined with chitosan features (CHIT/HPMCAS system) demonstrated a gastric peptide release of 3.59 ± 1.3%, which means a higher polycationic attraction, and consequently a greater acid pH-resistance. The high porosity of the alginate particles contributed to the quick release of the bioactive compound, which was accompanied by water solubility [87]. The Ctx peptide exhibited high solubility (Table S1), and this property allowed the design of a coating system with greater ionic interaction.

According to the r^2 values obtained from all the developed samples (Table 4), it can be concluded that the Ctx peptide release in both release solutions tested (SGF and SIF) was governed by the Korsmeyer-Peppas mathematical model. This model is based on the Power Law and exponentially relates the release of the drug (Mt/M∞) to time (t) (Equation (3)):

$$\frac{M_t}{M_\infty} = kt^n \quad (3$$

where M is the mass fraction of the peptide released with respect to time and can provide information on the release mechanism through the release exponent (n).

All samples yielded a value of $n < 0.43$ (for spherical dosage forms), which indicates that the low release rates observed in an acid medium occurred by Fickian diffusion, that is, according to a concentration gradient. On the other hand, there were different n-values in the simulated intestinal environment, except for the CHIT sample ($n = 0.4096$), which also exhibited a release rate governed by Fickian diffusion, although the release of the Ctx peptide through the CHIT sample also had a good correlation with the first-order models ($r^2 = 0.8329$) and Hixson-Crowell ($r^2 = 0.8696$) [88]. It is known that the first-order model has been applied mainly to porous systems containing hydrophilic drugs, while the Hixson-Crowell model is applicable to systems showing changes in surface area and particle diameter. This behavior is not consistent with the composition of the sample, since chitosan has its solubility drastically reduced in media with a pH from neutral to basic, presenting no changes in dimension due to the absorption of the simulated solution [89].

In contrast, the HPMCAS-coated sample had n values between 0.43 and 0.85 ($n = 0.8091$), which indicates that the release was directed by non-Fickian diffusion, that is, an anomalous transport implied in the relaxation of HPMCAS polymeric chains due to its high solubility in media with intestinal pH. Finally, a value of n greater than 0.85 was

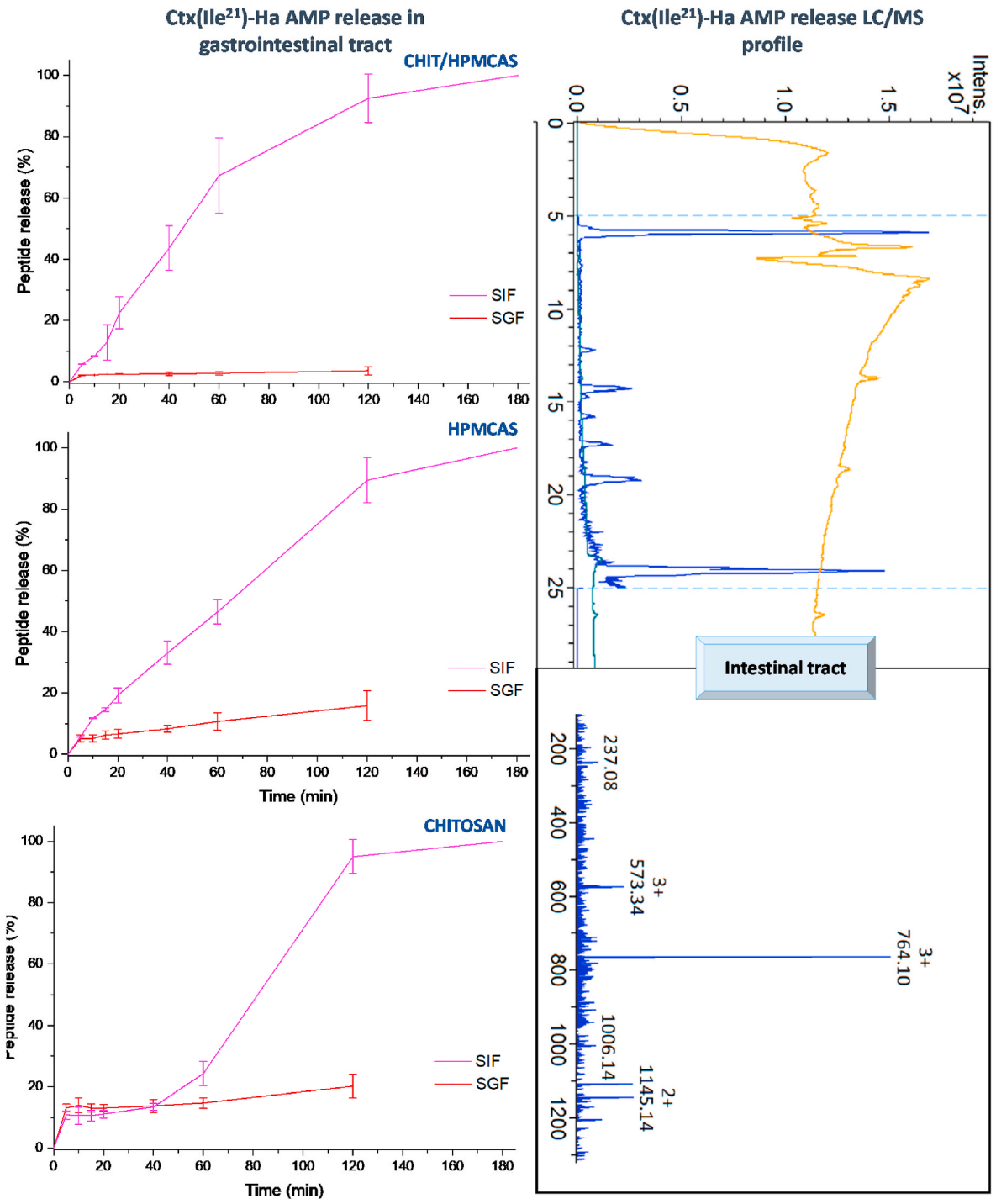

Fig. 6. *In vitro* release in the gastrointestinal tract (GIT) of the different systems developed. The left side shows the different systems that were synthesized and placed in SGF (gastric) and SIF (intestinal) GIT solutions. The collected aliquots were read at different times simulating the normal pathway of oral drugs in human GIT. The right side shows the chromatographic-mass spectrometry (blue line) and UV (orange line) profile, revealing the identity of the Ctx(Ile^{21})-Ha AMP. (For interpretation of the references to color in this figure legend, the reader is referred to the Web version of this article.)

verified for the CHIT/HPMCAS sample ($n = 1.1080$), which suggests a super case-II transport. This transport occurs when sorption is fully controlled by stress-induced relaxations [90], demonstrating the influence of both polymeric hydration and swelling, which may also be related to alginate matrix erosion [91].

3.5. *In vitro* enzymatic inhibition results

The proteolytic activity of gastric and intestinal enzymes was evaluated, using as reference the Ctx controlled release results as 100% of the peptide content in the simulated fluid. Enzymatic degradation against the pure Ctx peptide became evident during the release over time. Based on the 100% release of SGF (previous section), Fig. 7 was designed to quantitatively analyze the amount of AMP degraded over time. In the CHIT system, it was observed that the level of protection offered by the chitosan coating was limited to a period of 120 min, which gradually degraded as the peptide was released. This occurred because chitosan is highly soluble under acidic conditions and easily

Table 4
Mathematical study of *in vitro* release values. The release constants of each material model and their comparison between the simulated SGF and SIF solutions are described.

Release model	SGF samples				SIF samples			
		CHIT	**HPMCAS**	**CHIT/HPMCAS**		**CHIT**	**HPMCAS**	**CHIT/HPMCAS**
Baker-Lonsdale	***k***	0.00009	0.00004	0.000003	***k***	0.0008	0.0011	0.0013
	r^2	0.3082	0.9653	0.4024	r^2	0.6827	0.8491	0.8629
Higuchi	***k***	2.2365	1.4492	0.4047	***k***	6.3505	6.8513	7.4277
	r^2	0.2592	0.9632	0.3942	r^2	0.7530	0.9166	0.9208
Korsmeyer-Peppas	***k***	**9.4651**	**1.8953**	**1.5307**	***k***	**3.8382**	**1.6866**	**0.7373**
	r^2	**0.9214**	**0.9696**	**0.9692**	r^2	**0.8117**	**0.9989**	**0.9883**
	n	**0.1321**	**0.4301**	**0.1624**	***n***	**0.4096**	**0.8091**	**1.1080**
First-order	***k***	–	0.0017	–	***k***	0.0104	0.0128	0.0160
	r^2	0	0.5569	0	r^2	0.8329	0.9679	0.9776
Hixson- Crowell	***k***	–	0.0006	–	***k***	0.0031	0.0036	0.0046
	r^2	0	0.5395	0	r^2	0.8696	0.9879	0.9911
Weibull	*k*	14.7694	21.6191	3.7705	***k***	29.8225	38.2000	50.4777
	r^2	0.7687	0.9196	0.7995	r^2	0.6236	0.9989	0.9779
	b	0.5563	0.5751	0.5161	***b***	0.5802	0.8392	0.0145

k = release constant; r^2 = coefficient of determination; n = release exponent; b = b parameter of Weibull.

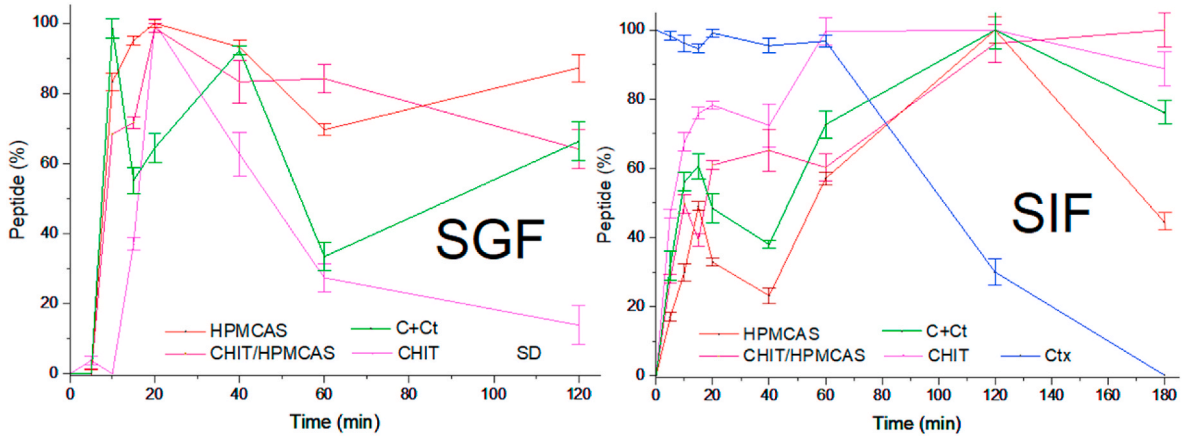

Fig. 7. Release and percentage quantification of the Ctx(Ile^{21})-Ha in SGF and SIF solutions.

dissolves, losing the coating protection.

Studies on the SIF using pancreatin (lipase + amylase + protease from porcine pancreas) were compared, and it was observed that the Ctx degradation occurred after 1 h, which made the peptide slightly tolerant to proteases. However, its action could be affected in later times due to its digestion. In contrast to encapsulated and coated systems, there is greater tolerance and resistance due to the alginate networks formed during cross-linking. In addition, the temporary chelating effect of HPMCAS (due to the carboxyl groups) could prevent the action of these enzymes during the Ctx release and action [92]. In addition, previous studies indicated that chitosan could be degraded by the presence of pancreatin lipase. However, this event can be temporarily paused due to the chelating effect provided by carboxyl groups of HPMCAS and alginate, capturing Mg^{2+}, Ca^{2+} and Mn^{2+} ions at intestinal pH [93]. Therefore, the combined use of HPMCAS, chitosan, and alginate polymers benefits the delivery and physicochemical stability of the Ctx peptide.

3.6. Antimicrobial activity prediction in drug delivery

Lysed bacteria were predicted as a function of the release peptide concentration using MIC values (Table 1), employing the McFarland scale and SIF release (%) *in vitro* verified from each system (Fig. 7). The bacterial number, expressed in colony-forming units (CFU) per mL, was obtained as a function of time (Fig. 8). It is worth mentioning that this AA is only a prediction, since these values could be increased by the AA that chitosan [94] and the alginate/chitosan combination intrinsically demonstrate [95]. Additionally, chitosan has been reported to promote wound healing of both skin tissue and intestine, which could be beneficial when it comes to diseases caused by hemorrhagic gut bacteria [96,97].

3.7. Cytotoxic activity

The activity in Caco-2 cells allowed us to verify whether the coated microparticles alter the viability in the intestine or colon. These results showed that none of the formulations are capable of inhibiting their viability or lysing the cells, and only the pure peptide at a concentration of 1 mg/mL was capable of lysing the cells. These results agree with other micro/nanoparticle systems based on alginate [98,99], chitosan [100–102], and HPMCAS [16,103] previously reported. Fig. 9 shows the cellular inhibition values of the peptide, and the cell viability of the double-coated alginate microparticles is highlighted, allowing us to deduce that they are not cytotoxic and that they are reliable for their antimicrobial action throughout the intestinal region [104].

In summary, the structural approach is important because it helps to understand the affinity and improve the peptide interaction with the desired receptor. For this reason, it is important to expand the present study with a wide gamma of relevant molecules from several infectious bacteria and more sophisticated approaches like molecular dynamics simulations and free energy calculations. Finally, these findings meet the basic conditions of physicochemical stability of microparticles with

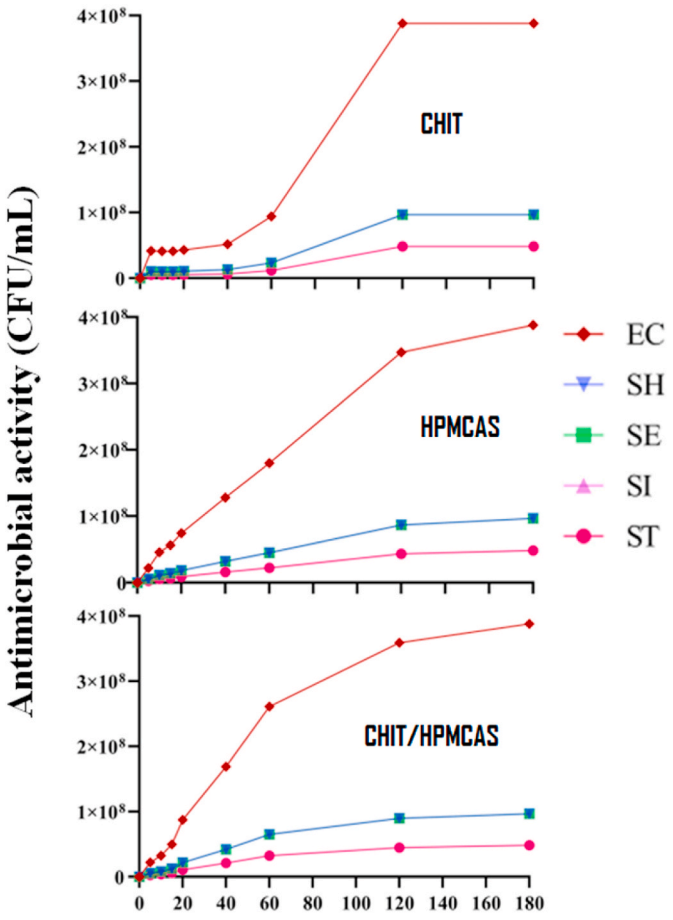

Fig. 8. Correlation between antimicrobial activity and SIF for each system. The bacterial inhibition concentration was calculated using the concentration values of the peptide released in the SIF at different times (5, 10, 20, 40, 60, 120, and 180 min) and the MIC values.

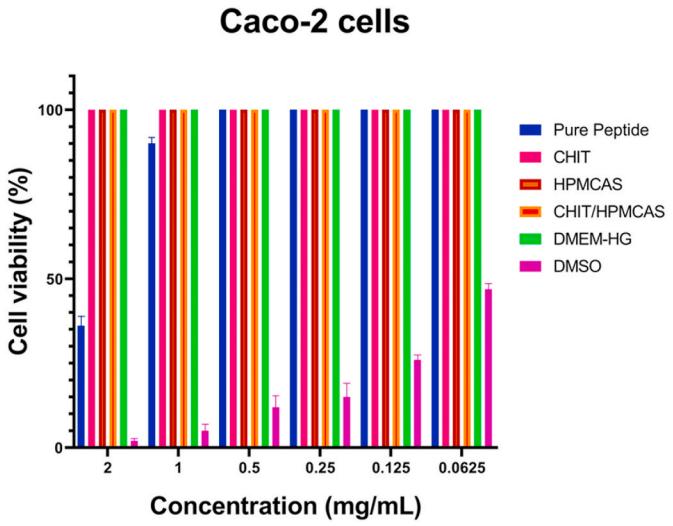

Fig. 9. Cell viability in Caco-2 cells after 24 h of treatment exposed to coated microparticles at 37 °C and 5% CO_2. The procedures were performed in triplicate and under aseptic conditions.

potential antibacterial activity, digestive release conditions, and stability against proteolytic enzymes. Furthermore, it was previously demonstrated that alginate-based microparticles can cross the intestinal barrier, preventing systemic infection caused by intestinal and colonic pathogens [16].

4. Conclusions

The Ctx(Ile^{21})-Ha AMP showed great activity against the pathogenic bacteria that cause infectious diseases, such as *Salmonella* spp. and *E. coli*. Thus, the use of this molecule as a food additive can be interesting, since AMP poses a minimal risk of bacterial resistance. CHIT/HPMCAS systems showed rigorous gastric protection during *in vitro* transport in the GIT, followed by HPMCAS and subsequently CHIT-coated system. Overall, these results allowed us to conclude that this bilayer microparticle system could be used to protect AMP or other bioactive compounds that are acidic pH sensitive. Therefore, the present study can substantially impact the development of new pharmaceutical and food formulations that help combat and prevent intestinal infection.

Credit author statement

Cesar Augusto Roque Borda: Writing - original draft, Investigation, results analysis and evaluation of the employed techniques. **José C. E. Márquez Montesinos:** Bioinformatic analyses. **Anna Beatriz Toledo Borges:** peptide synthesis and microencapsulation. **Edson Crusca Junior, Saulo Santesso Garrido, Reinaldo Marchetto:** analytical HPLC profile and peptide characterization. **Andréia Bagliotti Meneguin and Marlus Chorilli:** encapsulation and coating process design. **Wagner Costa Macedo and Silvio Rainho Teixeira:** microparticles characterization by DSC/TGA and XRD. **Adriana Maria de Almeida, Angelo Berchieri Junior, Mauro de Mesquita Souza Saraiva and Fernando Rogerio Pavan:** Cytotoxic studies, antibacterial analysis and article review. **Eduardo Festozo Vicente:** Conceptualization, Development, Supervision, Funding acquisition, article review and writing.

Declaration of competing interest

The authors declare that they have no known competing financial interests or personal relationships that could have appeared to influence the work reported in this paper.

Data availability

Data will be made available on request.

Acknowledgments

This work was developed with the support of São Paulo Research Foundation/FAPESP (Fundação de Amparo à Pesquisa do Estado de São Paulo, Proc. Number 2016/00446–7) and scholarships (Proc. Number 2018/25707–3 and 2020/16573–3). We thank the technical assistants of the Chemistry and Biochemistry Laboratory from FCE/Unesp Tupã, Institute of Chemistry, Araraquara (IQ-Unesp), for the use of LC/MS equipment, Shin-Etsu Chemical Co., Ltd. for kindly providing the coating (HPMCAS) for the experiments, and the research group "Peptides: Synthesis, Optimization and Applied Studies - PeSEAp". We also thank the Ultrastructure Celular Laboratory, Carlos Alberto Redins (LUCCAR), CCS/UFES, MCT/FINEP/CT-INFRA – PROINFRA 01/2006 for the SEM images. Special thanks to the researchers Daniel F. Monte and Valdinete Pereira Benevides from FCAV/Unesp for their support and collaboration in MIC studies.

Appendix A. Supplementary data

Supplementary data to this article can be found online at https://doi.org/10.1016/j.biomaterials.2022.121978.

References

[1] W.H.O., WHO, Salmonella (non-typhoidal) (2018) accessed January 5, 2021, https://www.who.int/news-room/fact-sheets/detail/salmonella-(non-typhoidal).

[2] C.A. Roque-Borda, P. Bento, da Silva, M.C. Rodrigues, R.B. Azevedo, L. Di Filippo, J.L. Duarte, M. Chorilli, E. Festozo Vicente, F.R. Pavan, Challenge in the discovery of new drugs: antimicrobial peptides against WHO-list of critical and high-priority bacteria, Pharmaceutics 13 (2021) 773, https://doi.org/10.3390/pharmaceutics13060773.

[3] E. Tacconelli, E. Carrara, A. Savoldi, S. Harbarth, M. Mendelson, D.L. Monnet, C. Pulcini, G. Kahlmeter, J. Kluytmans, Y. Carmeli, M. Ouellette, K. Outterson, J. Patel, M. Cavaleri, E.M. Cox, C.R. Houchens, M.L. Grayson, P. Hansen, N. Singh, U. Theuretzbacher, N. Magrini, A.O. Aboderin, S.S. Al-Abri, N. Awang Jalil, N. Benzonana, S. Bhattacharya, A.J. Brink, F.R. Burkert, O. Cars, G. Cornaglia, O.J. Dyar, A.W. Friedrich, A.C. Gales, S. Gandra, C.G. Giske, D. A. Goff, H. Goossens, T. Gottlieb, M. Guzman Blanco, W. Hryniewicz, D. Kattula, T. Jinks, S.S. Kanj, L. Kerr, M.P. Kieny, Y.S. Kim, R.S. Kozlov, J. Labarca, R. Laxminarayan, K. Leder, L. Leibovici, G. Levy-Hara, J. Littman, S. Malhotra-Kumar, V. Manchanda, L. Moja, B. Ndoye, A. Pan, D.L. Paterson, M. Paul, H. Qiu, P. Ramon-Pardo, J. Rodríguez-Baño, M. Sanguinetti, S. Sengupta, M. Sharland, M. Si-Mehand, L.L. Silver, W. Song, M. Steinbakk, J. Thomsen, G.E. Thwaites, J. W. van der Meer, N. Van Kinh, S. Vega, M.V. Villegas, A. Wechsler-Fördös, H.F. L. Wertheim, E. Wesangula, N. Woodford, F.O. Yilmaz, A. Zorzet, Discovery, research, and development of new antibiotics: the WHO priority list of antibiotic-resistant bacteria and tuberculosis, Lancet Infect. Dis. 18 (2018) 318–327, https://doi.org/10.1016/S1473-3099(17)30753-3.

[4] S. Mankoci, J. Ewing, P. Dalai, N. Sahai, H.A. Barton, A. Joy, Bacterial membrane selective antimicrobial peptide-mimetic polyurethanes: structure–property correlations and mechanisms of action, Biomacromolecules 20 (2019) 4096–4106, https://doi.org/10.1021/acs.biomac.9b00939.

[5] J. Bo, Y. Yang, R. Zheng, C. Fang, Y. Jiang, J. Liu, M. Chen, F. Hong, C. Bailey, H. Segner, K. Wang, Antimicrobial activity and mechanisms of multiple antimicrobial peptides isolated from rockfish Sebastiscus marmoratus, Fish Shellfish Immunol. 93 (2019) 1007–1017, https://doi.org/10.1016/j.fsi.2019.08.054.

[6] L.M. Gottler, A. Ramamoorthy, Structure, membrane orientation, mechanism, and function of pexiganan — a highly potent antimicrobial peptide designed from magainin, Biochim. Biophys. Acta Biomembr. 1788 (2009) 1680–1686, https://doi.org/10.1016/j.bbamem.2008.10.009.

[7] J.T.C. de Pontes, A.B. Toledo Borges, C.A. Roque-Borda, F.R. Pavan, Antimicrobial peptides as an alternative for the eradication of bacterial biofilms of multi-drug resistant bacteria, Pharmaceutics 14 (2022) 642, https://doi.org/10.3390/pharmaceutics14030642.

[8] A. Ye, J. Cui, H. Singh, Proteolysis of milk fat globule membrane proteins during in vitro gastric digestion of milk, J. Dairy Sci. 94 (2011) 2762–2770, https://doi.org/10.3168/jds.2010-4099.

[9] A. Bratovcic, J. Suljagic, Micro- and nano-encapsulation in food industry, Croat, J. Food Sci. Technol. 11 (2019) 113–121, https://doi.org/10.17508/cjfst.2019.11.1.17.

[10] B. Wang, Y. Wan, Y. Zheng, X. Lee, T. Liu, Z. Yu, J. Huang, Y.S. Ok, J. Chen, B. Gao, Alginate-based composites for environmental applications: a critical review, Crit. Rev. Environ. Sci. Technol. 49 (2019) 318–356, https://doi.org/10.1080/10643389.2018.1547621.

[11] G.C. Avendaño-Romero, A. López-Malo, E. Palou, Propiedades del alginato y aplicaciones en alimentos, Temas Sel. Ing. Aliment. 7 (2013) 87–96.

[12] S. Kaur, R.K. Narang, G. Aggarwal, Formulation and development of colon-targeted mucopenetrating metronidazole nanoparticles, Trop. J. Pharmaceut. Res. 16 (2017) 967–973, https://doi.org/10.4314/tjpr.v16i5.1.

[13] I.A. Sogias, A.C. Williams, V.V. Khutoryanskiy, Why is chitosan mucoadhesive? Biomacromolecules 9 (2008) 1837–1842, https://doi.org/10.1021/bm800276d.

[14] P.S. Anbinder, L. Deladino, A.S. Navarro, J.I. Amalvy, M.N. Martino, Yerba mate extract encapsulation with alginate and chitosan systems: interactions between active compound encapsulation polymers, J. Encapsulation Adsorpt. Sci. 1 (2011) 80–87, https://doi.org/10.4236/jeas.2011.14011.

[15] C.A. Roque-Borda, H.R.L. Silva, E. Crusca Junior, J.A. Serafim, A.B. Meneguin, M. Chorilli, W.C. Macedo, S.R. Teixeira, E.A.L. Guastalli, N.M. Soares, J.M. Blair, Z. Pikramenou, E.F. Vicente, Alginate-based microparticles coated with HPMCP/AS cellulose-derivatives enable the Ctx(Ile21)-Ha antimicrobial peptide application as a feed additive, Int. J. Biol. Macromol. 183 (2021) 1236–1247, https://doi.org/10.1016/j.ijbiomac.2021.05.011.

[16] C.A. Roque-Borda, , M. de M. Souza Saraiva, D.F.M. Monte, L.B. Rodrigues Alves, A.M. de Almeida, T.S. Ferreira, T.S. de Lima, V.P. Benevides, J.M. Cabrera, S. Claire, A.B. Meneguin, M. Chorilli, F.R. Pavan, A.B. Junior, E.F. Vicente, HPMCAS-coated alginate microparticles loaded with ctx(ile 21)-Ha as a promising antimicrobial agent against Salmonella Enteritidis in a chicken infection model, ACS Infect. Dis. 8 (2022) 472–481, https://doi.org/10.1021/acsinfecdis.1c00264.

[17] G. Ferreira Cespedes, E. Nicolas Lorenzon, E. Festozo Vicente, M. Jose Soares Mendes-Giannini, W. Fontes, M. de Souza Castro, E. Maffud Cilli, Mechanism of action and relationship between structure and biological activity of ctx-ha: a new ceratotoxin-like peptide from hypsiboas albopunctatus, protein pept, Letture 19 (2012) 596–603, https://doi.org/10.2174/092986612800494011.

[18] E.F. Vicente, L.G.M. Basso, G.F. Cespedes, E.N. Lorenzón, M.S. Castro, M.J. S. Mendes-Giannini, A.J. Costa-Filho, E.M. Cilli, Dynamics and conformational studies of TOAC spin labeled analogues of ctx(ile21)-ha peptide from hypsiboas albopunctatus, PLoS One 8 (2013), e60818, https://doi.org/10.1371/journal.pone.0060818.

[19] E.N. Lorenzón, G.F. Cespedes, E.F. Vicente, L.G. Nogueira, T.M. Bauab, M. S. Castro, E.M. Cilli, Effects of dimerization on the structure and biological activity of antimicrobial peptide ctx-ha, antimicrob, Agents Chemother 56 (2012) 3004–3010, https://doi.org/10.1128/AAC.06262-11.

[20] Y. Fan, Z. Yu, W. Zhao, L. Ding, F. Zheng, J. Li, J. Liu, Identification and molecular mechanism of angiotensin-converting enzyme inhibitory peptides from Larimichthys crocea titin, Food Sci. Hum. Wellness 9 (2020) 257–263, https://doi.org/10.1016/J.FSHW.2020.04.001.

[21] A. Lamiable, P. Thévenet, J. Rey, M. Vavrusa, P. Derreumaux, P. Tufféry, PEP-FOLD3: faster de novo structure prediction for linear peptides in solution and in complex, Nucleic Acids Res. 44 (2016) W449–W454, https://doi.org/10.1093/nar/gkw329.

[22] J. Maupetit, P. Tuffery, P. Derreumaux, A coarse-grained protein force field for folding and structure prediction, Proteins: Struct., Funct., Bioinf. 69 (2007) 394–408, https://doi.org/10.1002/prot.21505.

[23] W. Humphrey, A. Dalke, K. Schulten, VMD: Visual molecular dynamics, J. Mol. Graph. 14 (1996) 33–38, https://doi.org/10.1016/0263-7855(96)00018-5.

[24] H.M. Berman, The protein data bank, Nucleic Acids Res. 28 (2000) 235–242, https://doi.org/10.1093/nar/28.1.235.

[25] P.T. Lang, S.R. Brozell, S. Mukherjee, E.F. Pettersen, E.C. Meng, V. Thomas, R. C. Rizzo, D.A. Case, T.L. James, I.D. Kuntz, Dock 6: combining techniques to model RNA–small molecule complexes, RNA 15 (2009) 1219–1230, https://doi.org/10.1261/rna.1563609.

[26] D.T. Moustakas, P.T. Lang, S. Pegg, E. Pettersen, I.D. Kuntz, N. Brooijmans, R. C. Rizzo, Development and validation of a modular, extensible docking program: dock 5, J. Comput. Aided Mol. Des. 20 (2006) 601–619, https://doi.org/10.1007/s10822-006-9060-4.

[27] E.F. Pettersen, T.D. Goddard, C.C. Huang, G.S. Couch, D.M. Greenblatt, E. C. Meng, T.E. Ferrin, UCSF Chimera?A visualization system for exploratory research and analysis, J. Comput. Chem. 25 (2004) 1605–1612, https://doi.org/10.1002/jcc.20084.

[28] J. Roel-Touris, B. Jiménez-García, A.M.J.J. Bonvin, Integrative modeling of membrane-associated protein assemblies, Nat. Commun. 11 (2020) 6210, https://doi.org/10.1038/s41467-020-20076-5.

[29] J. Roel-Touris, A.M.J.J. Bonvin, B. Jiménez-García, LightDock goes information-driven, Bioinformatics 36 (2020) 950–952, https://doi.org/10.1093/bioinformatics/btz642.

[30] B. Jiménez-García, J. Roel-Touris, M. Romero-Durana, M. Vidal, D. Jiménez-González, J. Fernández-Recio, LightDock: a new multi-scale approach to protein–protein docking, Bioinformatics 34 (2018) 49–55, https://doi.org/10.1093/bioinformatics/btx555.

[31] K.N. Krishnanand, D. Ghose, Glowworm swarm optimization for simultaneous capture of multiple local optima of multimodal functions, Swarm Intell 3 (2009) 87–124, https://doi.org/10.1007/s11721-008-0021-5.

[32] S. Liu, C. Zhang, H. Zhou, Y. Zhou, A physical reference state unifies the structure-derived potential of mean force for protein folding and binding, Proteins: Struct., Funct., Bioinf. 56 (2004) 93–101, https://doi.org/10.1002/prot.20019.

[33] M.F. Adasme, K.L. Linnemann, S.N. Bolz, F. Kaiser, S. Salentin, V.J. Haupt, M. Schroeder, Plip 2021: expanding the scope of the protein–ligand interaction profiler to DNA and RNA, Nucleic Acids Res. 49 (2021) W530–W534, https://doi.org/10.1093/nar/gkab294.

[34] C. Mooney, N.J. Haslam, G. Pollastri, D.C. Shields, Towards the improved discovery and design of functional peptides: common features of diverse classes permit generalized prediction of bioactivity, PLoS One 7 (2012), e45012, https://doi.org/10.1371/JOURNAL.PONE.0045012.

[35] S. Gupta, P. Kapoor, K. Chaudhary, A. Gautam, R. Kumar, O.S.D.D. Consortium, G.P.S. Raghava, In silico approach for predicting toxicity of peptides and proteins, PLoS One 8 (2013), e73957, https://doi.org/10.1371/JOURNAL.PONE.0073957.

[36] E. Gasteiger, C. Hoogland, A. Gattiker, S. Duvaud, M.R. Wilkins, R.D. Appel, A. Bairoch, Protein identification and analysis tools on the ExPASy server, in: Springer (Ed.), Proteomics Protoc. Handb., Humana Press, Totowa, NJ, 2005, pp. 571–607, https://doi.org/10.1385/1-59259-890-0:571.

[37] F. Li, A. Leier, Q. Liu, Y. Wang, D. Xiang, T. Akutsu, G.I. Webb, A.I. Smith, T. Marquez-Lago, J. Li, J. Song, Procleave: predicting protease-specific substrate cleavage sites by combining sequence and structural information, genomics, Proteomics Bioinformatics 18 (2020) 52–64, https://doi.org/10.1016/j.gpb.2019.08.002.

[38] G. Xiong, Z. Wu, J. Yi, L. Fu, Z. Yang, C. Hsieh, M. Yin, X. Zeng, C. Wu, A. Lu, X. Chen, T. Hou, D. Cao, ADMETlab 2.0: an integrated online platform for accurate and comprehensive predictions of ADMET properties, Nucleic Acids Res. 49 (2021) W5–W14, https://doi.org/10.1093/NAR/GKAB255.

[39] N. Rezaei, F. Mehrnejad, Z. Vaezi, M. Sedghi, S.M. Asghari, H. Naderi-Manesh, Encapsulation of an endostatin peptide in liposomes: stability, release, and cytotoxicity study, Colloids Surf., B 185 (2020), 110552, https://doi.org/10.1016/j.colsurfb.2019.110552.

[40] M. Krewing, B. Schubert, J.E. Bandow, A dielectric barrier discharge plasma degrades proteins to peptides by cleaving the peptide bond, Plasma Chem. Plasma Process. 403 (40) (2019) 685–696, https://doi.org/10.1007/S11090-019-10053-2, 2019.

[41] S. Park, J.O. Baker, M.E. Himmel, P.A. Parilla, D.K. Johnson, Cellulose crystallinity index: measurement techniques and their impact on interpreting cellulase performance, Biotechnol. Biofuels 3 (2010) 10, https://doi.org/10.1186/1754-6834-3-10.

[42] Y. Zhang, C. Xue, Z. Li, Y. Zhang, X. Fu, Preparation of half-deacetylated chitosan by forced penetration and its properties, Carbohydr, Polym 65 (2006) 229–234, https://doi.org/10.1016/j.carbpol.2005.08.066.

[43] Y. Zhang, R. Remadevi, J.P. Hinestroza, X. Wang, M. Naebe, Transparent ultraviolet (UV)-shielding films made from waste hemp hurd and polyvinyl alcohol (PVA), Polymers 12 (2020), https://doi.org/10.3390/POLYM12051190.

[44] C.L.S.I.P. standards, For Antimicrobial Susceptibility Testing CLSI, M100 Performance Standards for Antimicrobial Susceptibility Testing, 28th ed., 2018 accessed March 12, 2021, www.clsi.org.

[45] A.B. Meneguin, E. Beyssac, G. Garrait, H. Hsein, B.S.F. Cury, Retrograded starch/pectin coated gellan gum-microparticles for oral administration of insulin: a technological platform for protection against enzymatic degradation and improvement of intestinal permeability, Eur. J. Pharm. Biopharm. 123 (2018) 84–94, https://doi.org/10.1016/j.ejpb.2017.11.012.

[46] R.A. De Grandis, K.M. Oliveira, A.P.M. Guedes, P.W.S. dos Santos, A.F. Aissa, A. A. Batista, F.R. Pavan, A novel ruthenium(II) complex with lapachol induces G2/M phase arrest through aurora-B kinase down-regulation and ROS-mediated apoptosis in human prostate adenocarcinoma cells, Front. Oncol. 11 (2021), https://doi.org/10.3389/fonc.2021.682968.

[47] C.A. Roque-Borda, L.P. Pereira, E.A.L. Guastalli, N.M. Soares, P.A.B. Mac-Lean, D. D. Salgado, A.B. Meneguin, M. Chorilli, E.F. Vicente, HPMCP-coated microcapsules containing the ctx(ile21)-ha antimicrobial peptide reduce the mortality rate caused by resistant Salmonella Enteritidis in laying hens, Antibiotics 10 (2021) 616, https://doi.org/10.3390/antibiotics10060616.

[48] C. Zhang, S. Liu, Q. Zhu, Y. Zhou, A knowledge-based energy function for Protein−Ligand, Protein−Protein, and Protein−DNA complexes, J. Med. Chem. 48 (2005) 2325–2335, https://doi.org/10.1021/jm049314d.

[49] S.J. Crennell, E.F. Garman, C. Philippon, A. Vasella, G.W. Laver, E.R. Vimr, G. L. Taylor, The structures ofSalmonella typhimuriumLT2 neuraminidase and its complexes with three inhibitors at high resolution, J. Mol. Biol. 259 (1996) 264–280, https://doi.org/10.1006/jmbi.1996.0318.

[50] J. Mehta, R. Rolta, K. Dev, Role of medicinal plants from North Western Himalayas as an efflux pump inhibitor against MDR AcrAB-TolC Salmonella enterica serovar typhimurium: in vitro and in silico studies, J. Ethnopharmacol. 282 (2022), 114589, https://doi.org/10.1016/j.jep.2021.114589.

[51] T. Rohand, H. Ben EL Ayouchia, H. Achtak, A. Ghaleb, Y. Derin, A. Tutar, K. Tanemura, Design, synthesis, DFT calculations, molecular docking and antimicrobial activities of novel cobalt, chromium metal complexes of heterocyclic moiety-based 1,3,4-oxadiazole derivatives, J. Biomol. Struct. Dyn. (2021) 1–14, https://doi.org/10.1080/07391102.2021.1965031.

[52] M. Song, S. Wang, Z. Wang, Z. Fu, S. Zhou, H. Cheng, Z. Liang, X. Deng, Synthesis, antimicrobial and cytotoxic activities, and molecular docking studies of N-arylsulfonylindoles containing an aminoguanidine, a semicarbazide, and a thiosemicarbazide moiety, Eur. J. Med. Chem. 166 (2019) 108–118, https://doi.org/10.1016/j.ejmech.2019.01.038.

[53] G.R. Dwivedi, A. Maurya, D.K. Yadav, V. Singh, F. Khan, M.K. Gupta, M. Singh, M.P. Darokar, S.K. Srivastava, Synergy of clavine alkaloid 'chanoclavine' with tetracycline against multi-drug-resistant E. coli, J. Biomol. Struct. Dyn. 37 (2019) 1307–1325, https://doi.org/10.1080/07391102.2018.1458654.

[54] M.M. Khalaf, H.M.A. El-Lateef, A. Alhadhrami, F.N. Sayed, G.G. Mohamed, M. Gouda, S. Shaaban, A.M. Abu-Dief, Synthesis, spectroscopic, structural and molecular docking studies of some new nano-sized ferrocene-based imine chelates as antimicrobial and anticancer agents, Materials 15 (2022) 3678, https://doi.org/10.3390/ma15103678.

[55] J.D. Irvine, L. Takahashi, K. Lockhart, J. Cheong, J.W. Tolan, H.E. Selick, J. R. Grove, MDCK (Madin–Darby canine kidney) cells: a tool for membrane permeability screening, J. Pharmacol. Sci. 88 (1999) 28–33, https://doi.org/10.1021/JS9803205.

[56] Y.E. Yun, A.N. Edginton, Evaluation of models for predicting pediatric fraction unbound in plasma for human health risk assessment, J. Toxicol. Environ. Health Part A Curr. Issues. 84 (2021) 67–83, https://doi.org/10.1080/15287394.2020.1835761/SUPPL_FILE/UTEH_A_1835761_SM5314.DOCX.

[57] A. Gunes, M.L. Dahl, Variation in CYP1A2 activity and its clinical implications: influence of environmental factors and genetic polymorphisms, Pharmacogenomics 9 (2008) 625–637, https://doi.org/10.2217/14622416.9.5.625.

[58] M.R. Botton, M. Whirl-Carrillo, A.L. Del Tredici, K. Sangkuhl, L.H. Cavallari, J.A. G. Agúndez, J. Duconge, M.T.M. Lee, E.L. Woodahl, K. Claudio-Campos, A. K. Daly, T.E. Klein, V.M. Pratt, S.A. Scott, A. Gaedigk, PharmVar GeneFocus: CYP2C19, Clin. Pharmacol. Ther. 109 (2021) 352–366, https://doi.org/10.1002/CPT.1973.

[59] P.J. Wedlund, The CYP2C19 enzyme polymorphism, Pharmacology 61 (2000) 174–183, https://doi.org/10.1159/000028398.

[60] R.E. Cian, A. Campos-Soldini, L. Chel-Guerrero, S.R. Drago, D. Betancur-Ancona, Bioactive Phaseolus lunatus peptides release from maltodextrin/gum Arabic microcapsules obtained by spray drying after simulated gastrointestinal digestion, Int. J. Food Sci. Technol. 54 (2019) 2002–2009, https://doi.org/10.1111/IJFS.14031.

[61] H. Yoon, E.J. Dell, J.L. Freyer, L.M. Campos, W.D. Jang, Polymeric supramolecular assemblies based on multivalent ionic interactions for biomedical applications, Polymer (Guildf) 55 (2014) 453–464, https://doi.org/10.1016/j.polymer.2013.12.038.

[62] O. Gåserød, O. Smidsrød, G. Skjåk-Bræk, Microcapsules of alginate-chitosan - I. A quantitative study of the interaction between alginate and chitosan, Biomaterials 19 (1998) 1815–1825, https://doi.org/10.1016/S0142-9612(98)00073-8.

[63] R. Huang, X. Zhou, X. Liu, Q. Zhang, H. Jin, X. Shi, W. Luo, H. Deng, Nanofibrous mats layer-by-layer assembled by HTCC/Layered silicate composites with in vitro antitumor activity against SMMC-7721 cells, J. Biomed. Nanotechnol. 10 (2014) 485–499, https://doi.org/10.1166/jbn.2014.1716.

[64] A. Abdulkhani, A. Najd Mazhar, S. Hedjazi, Y. Hamzeh, Preparation of xylan bio-composite films reinforced with oxidized carboxymethyl cellulose and nanocellulose, Polym. Bull. 77 (2020) 6227–6239, https://doi.org/10.1007/s00289-019-03075-5.

[65] G. Güler, E. Džafić, M.M. Vorob'Ev, V. Vogel, W. Mäntele, Real time observation of proteolysis with Fourier transform infrared (FT-IR) and UV-circular dichroism spectroscopy: watching a protease eat a protein, Spectrochim. Acta Part A Mol. Biomol. Spectrosc. 79 (2011) 104–111, https://doi.org/10.1016/J.SAA.2011.01.055.

[66] T.M. Deshpande, A. Quadir, S. Obara, S.W. Hoag, Impact of formulation excipients on the thermal, mechanical, and electrokinetic properties of hydroxypropyl methylcellulose acetate succinate (HPMCAS), Int. J. Pharm. 542 (2018) 132–141, https://doi.org/10.1016/j.ijpharm.2018.02.024.

[67] X. Chen, I. Partheniadis, I. Nikolakakis, H. Al-Obaidi, Solubility improvement of progesterone from solid dispersions prepared by solvent evaporation and Co-milling, Polym 12 (2020) 854, https://doi.org/10.3390/POLYM12040854, 12 (2020) 854.

[68] J. Nunthanid, K. Huanbutta, M. Luangtana-anan, P. Sriamornsak, S. Limmatvapirat, S. Puttipipatkhachorn, Development of time-, pH-, and enzyme-controlled colonic drug delivery using spray-dried chitosan acetate and hydroxypropyl methylcellulose, Eur. J. Pharm. Biopharm. 68 (2008) 253–259, https://doi.org/10.1016/j.ejpb.2007.05.017.

[69] C.H. Tang, Z. Chen, L. Li, X.Q. Yang, Effects of transglutaminase treatment on the thermal properties of soy protein isolates, Food Res. Int. 39 (2006) 704–711, https://doi.org/10.1016/j.foodres.2006.01.012.

[70] R.P. Aquino, G. Auriemma, M. D'Amore, A.M. D'Ursi, T. Mencherini, P. Del Gaudio, Piroxicam loaded alginate beads obtained by prilling/microwave tandem technique: morphology and drug release, Carbohydr, Polym 89 (2012) 740–748, https://doi.org/10.1016/j.carbpol.2012.04.003.

[71] S.M. Hosseini, H. Hosseini, M.A. Mohammadifar, J.B. German, A.M. Mortazavian, A. Mohammadi, K. Khosravi-Darani, S. Shojaee-Aliabadi, R. Khaksar, Preparation and characterization of alginate and alginate-resistant starch microparticles containing nisin, Carbohydr. Polym. 103 (2014) 573–580, https://doi.org/10.1016/j.carbpol.2013.12.078.

[72] J.B.E. Mendes, M.K. Riekes, V.M. De Oliveira, M.D. Michel, H.K. Stulzer, N. M. Khalil, S.F. Zawadzki, R.M. Mainardes, P.V. Farago, PHBV/PCL microparticles for controlled release of resveratrol: physicochemical characterization, antioxidant potential, and effect on hemolysis of human erythrocytes, Sci. World J. (2012), https://doi.org/10.1100/2012/542937, 2012.

[73] L. Wang, Y. Ding, X. Zhang, Y. Li, R. Wang, X. Luo, Y. Li, J. Li, Z. Chen, Isolation of a novel calcium-binding peptide from wheat germ protein hydrolysates and the prediction for its mechanism of combination, Food Chem. 239 (2018) 416–426, https://doi.org/10.1016/J.FOODCHEM.2017.06.090.

[74] C. Zhang, X. Yang, W. Hu, X. Han, L. Fan, S. Tao, Preparation and characterization of carboxymethyl chitosan/collagen peptide/oxidized konjac composite hydrogel, Int. J. Biol. Macromol. 149 (2020) 31–40, https://doi.org/10.1016/J.IJBIOMAC.2020.01.127.

[75] S. Sharma, P. Sanpui, A. Chattopadhyay, S.S. Ghosh, Fabrication of antibacterial silver nanoparticle - sodium alginate-chitosan composite films, RSC Adv. 2 (2012) 5837–5843, https://doi.org/10.1039/c2ra00006g.

[76] J. Nunthanid, M. Laungtana-Anan, P. Sriamornsak, S. Limmatvapirat, S. Puttipipatkhachorn, L.Y. Lim, E. Khor, Characterization of chitosan acetate as a binder for sustained release tablets, J. Contr. Release 99 (2004) 15–26, https://doi.org/10.1016/j.jconrel.2004.06.008.

[77] C.T.M. Tran, P.H.L. Tran, T.T.D. Tran, pH-independent dissolution enhancement for multiple poorly water-soluble drugs by nano-sized solid dispersions based on hydrophobic–hydrophilic conjugates, Drug Dev. Ind. Pharm. 45 (2019) 514–519, https://doi.org/10.1080/03639045.2018.1562466.

[78] K. Tiseo, L. Huber, M. Gilbert, T.P. Robinson, T.P. Van Boeckel, Global trends in antimicrobial use in food animals from 2017 to 2030, Antibiotics 9 (2020) 918, https://doi.org/10.3390/antibiotics9120918.

[79] M.M.S. Saraiva, A.L.B. Moreira Filho, O.C. Freitas Neto, N.M.V. Silva, P.E. N. Givisiez, W.A. Gebreyes, C.J.B. Oliveira, Off-label use of ceftiofur in one-day chicks triggers a short-term increase of ESBL-producing E. coli in the gut, PLoS One 13 (2018), e0203158, https://doi.org/10.1371/journal.pone.0203158.

[80] C.M. Silva, A.J. Ribeiro, M. Figueiredo, D. Ferreira, F. Veiga, Microencapsulation of hemoglobin in chitosan-coated alginate microspheres prepared by emulsification/internal gelation, AAPS J. 7 (2006), https://doi.org/10.1208/aapsj070488.

[81] R. Arshady, Microcapsules for food, J. Microencapsul. 10 (1993) 413–435, https://doi.org/10.3109/02652049309015320.

[82] M. Fu, J.A. Blechar, A. Sauer, J. Al-Gousous, P. Langguth, In vitro evaluation of enteric-coated HPMC capsules—effect of formulation factors on product performance, Pharmaceutics 12 (2020) 696, https://doi.org/10.3390/pharmaceutics12080696.

[83] S. Surini, K. Prakoso, Preparation and characterization of chitosan succinate as coating polymer for enteric-coated tablet, Int. J. Appl. Pharm. 10 (2018) 343–347, https://doi.org/10.22159/ijap.2018.v10s1.76.

[84] H.J. Park, G.H. Lee, J.H. Jun, M. Son, Y.S. Choi, M.K. Choi, M.J. Kang, Formulation and in vivo evaluation of probiotics-encapsulated pellets with hydroxypropyl methylcellulose acetate succinate (HPMCAS), Carbohydr, Polym 136 (2015) 692–699, https://doi.org/10.1016/j.carbpol.2015.09.083.

[85] M.A. Momoh, P.A. Akpa, K.C. Ugwu, F.C. Kenechukwu, O.C. Kenneth, Pharmacodynamics and pharmacokinetics behaviour of insulin from PEGylated-mucin microparticles coated with pH sensitive polymer: preparation and characterization, Mater. Today Commun. 25 (2020), 101539, https://doi.org/10.1016/j.mtcomm.2020.101539.

[86] B. Kriwet, T. Kissel, Interactions between bioadhesive poly(acrylic acid) and calcium ions, Int. J. Pharm. 127 (1996) 135–145, https://doi.org/10.1016/0378-5173(95)04098-6.

[87] M. George, T.E. Abraham, pH sensitive alginate–guar gum hydrogel for the controlled delivery of protein drugs, Int. J. Pharm. 335 (2007) 123–129, https://doi.org/10.1016/J.IJPHARM.2006.11.009.

[88] H. Raslan, H. Maswadeh, In vitro dissolution kinetic study of theophylline from mixed controlled release matrix tablets containing hydroxypropylmethyl cellulose and glycerylbehenate, Indian J. Pharmaceut. Sci. 68 (2006) 308–312, https://doi.org/10.4103/0250-474X.26658.

[89] S. Dash, P.N. Murthy, L. Nath, P. Chowdhury, Kinetic modeling on drug release from controlled drug delivery systems, Acta Pol. Pharm. ñ Drug Res. 67 (2010) 217–223.

[90] C.H.M. Jacques, H.B. Hopfenberg, V. Stannett, Super Case II Transport of Organic Vapors in Glassy Polymers, 1974, pp. 73–86, https://doi.org/10.1007/978-1-4684-2877-3_6.

[91] S.R.P. Camelo, S. Franceschi, E. Perez, S.G. Fullana, M.I. Ré, Factors Influencing the Erosion Rate and the Drug Release Kinetics from Organogels Designed as Matrices for Oral Controlled Release of a Hydrophobic Drug vol. 42, 2015, pp. 985–997, https://doi.org/10.3109/03639045.2015.1103746. Https://Doi.Org/10.3109/03639045.2015.1103746.

[92] A. Dalmoro, A.A. Barba, G. Lamberti, M. Grassi, M. d'Amore, Pharmaceutical applications of biocompatible polymer blends containing sodium alginate, Adv. Polym. Technol. 31 (2012) 219–230, https://doi.org/10.1002/adv.21276.

[93] J. Lu, C.J. Brigham, C. Rha, A.J. Sinskey, Characterization of an extracellular lipase and its chaperone from Ralstonia eutropha H16, Appl. Microbiol. Biotechnol. 97 (2013) 2443–2454, https://doi.org/10.1007/s00253-012-4115-z.

[94] I. Bano, M. Arshad, T. Yasin, M.A. Ghauri, M. Younus, Chitosan: a potential biopolymer for wound management, Int. J. Biol. Macromol. 102 (2017) 380–383, https://doi.org/10.1016/j.ijbiomac.2017.04.047.

[95] M. Dumont, R. Villet, M. Guirand, A. Montembault, T. Delair, S. Lack, M. Barikosky, A. Crepet, P. Alcouffe, F. Laurent, L. David, Processing and antibacterial properties of chitosan-coated alginate fibers, Carbohydr. Polym. 190 (2018) 31–42, https://doi.org/10.1016/j.carbpol.2017.11.088.

[96] S. Vakilian, F. Jamshidi-adegani, A. Al Yahmadi, M. Al-Broumi, N. Ur Rehman, M. U. Anwar, K. Alam, N. Al-Wahaibi, A. Shalaby, S. Alyaqoobi, A. Al-Harrasi, K. Mustafa, S. Al-Hashmi, A competitive nature-derived multilayered scaffold based on chitosan and alginate, for full-thickness wound healing, Carbohydr. Polym. 262 (2021), https://doi.org/10.1016/j.carbpol.2021.117921.

[97] D. Xiao, Y. Wang, G. Liu, J. He, W. Qiu, X. Hu, Z. Feng, M. Ran, C.M. Nyachoti, S. W. Kim, Z. Tang, Y. Yin, Effects of chitosan on intestinal inflammation in weaned pigs challenged by enterotoxigenic Escherichia coli, PLoS One 9 (2014), e104192, https://doi.org/10.1371/JOURNAL.PONE.0104192.

[98] L. Long, M. Lai, X. Mao, J. Luo, X. Yuan, L.-M. Zhang, Z. Ke, L. Yang, D.Y. Deng, Investigation of vitamin B12-modified amphiphilic sodium alginate derivatives for enhancing the oral delivery efficacy of peptide drugs, Int. J. Nanomed. 14 (2019) 7743–7758, https://doi.org/10.2147/IJN.S218944.

[99] N. Goldberg, Y. Shmidov, O. Kryukov, D. Aranovich, S. Cohen, R. Bitton, Effect of heparin and peptide conjugation on structure and functional properties of alginate in solutions and hydrogels, Mater. Adv. 2 (2021) 440–447, https://doi.org/10.1039/D0MA00669F.

[100] H. Song, A. He, X. Guan, Z. Chen, Y. Bao, K. Huang, Fabrication of chitosan-coated epigallocatechin-3-gallate (EGCG)-hordein nanoparticles and their transcellular permeability in Caco-2/HT29 cocultures, Int. J. Biol. Macromol. 196 (2022) 144–150, https://doi.org/10.1016/j.ijbiomac.2021.12.024.

[101] Y. Zhao, W. Du, H. Wu, M. Wu, Z. Liu, S. Dong, Chitosan/sodium tripolyphosphate nanoparticles as efficient vehicles for enhancing the cellular uptake of fish-derived peptide, J. Food Biochem. 43 (2019), e12730, https://doi.org/10.1111/jfbc.12730.

[102] P. Batista, P.M. Castro, A.R. Madureira, B. Sarmento, M. Pintado, Preparation, characterization and evaluation of guar films impregnated with relaxing peptide loaded into chitosan microparticles, Appl. Sci. 11 (2021) 9849, https://doi.org/10.3390/app11219849.

[103] Z.-T. Lai, H.-B. Ding, Q.-Y. Jiang, Q.-L. Yuan, Z.-G. Liao, Effects of HPMCAS MF on absorption of silybin from supersaturable self-nanoemulsifying drug delivery system, Zhongguo Zhongyao Zazhi 46 (2021) 1120–1127, https://doi.org/10.19540/j.cnki.cjcmm.20201210.302.

[104] X. Ding, X. Hu, Y. Chen, J. Xie, M. Ying, Y. Wang, Q. Yu, Differentiated Caco-2 cell models in food-intestine interaction study: current applications and future trends, Trends Food Sci. Technol. 107 (2021) 455–465, https://doi.org/10.1016/j.tifs.2020.11.015.